

Photon-Number Dependent Hamiltonian Engineering for Cavities

Chiao-Hsuan Wang,^{1,*} Kyungjoo Noh,² José Lebreuilly,³ S. M. Girvin,³ and Liang Jiang¹

¹*Pritzker School of Molecular Engineering, University of Chicago, Chicago, Illinois 60637, USA*

²*AWS Center for Quantum Computing, Pasadena, California 91125, USA*

³*Department of Physics and Yale Quantum Institute, Yale University, New Haven, Connecticut 06520, USA*

Cavity resonators are promising resources for quantum technology, while native nonlinear interactions for cavities are typically too weak to provide the level of quantum control required to deliver complex targeted operations. Here we investigate a scheme to engineer a target Hamiltonian for photonic cavities using ancilla qubits. By off-resonantly driving dispersively coupled ancilla qubits, we develop an optimized approach to engineering an arbitrary photon-number dependent (PND) Hamiltonian for the cavities while minimizing the operation errors. The engineered Hamiltonian admits various applications including canceling unwanted cavity self-Kerr interactions, creating higher-order nonlinearities for quantum simulations, and designing quantum gates resilient to noise. Our scheme can be implemented with coupled microwave cavities and transmon qubits in superconducting circuit systems.

Microwave cavity resonators are rising as a promising platform for quantum information processing. Tremendous experimental progress has been made in building high-coherence microwave photon cavities in circuit quantum electrodynamics (cQED) platforms [1–4]. The infinite-dimensional Hilbert space of a single resonator enables flexible and hardware-efficient design of quantum error correction codes [5–10] and has led to the first success in extending logical qubit lifetime [11]. Controllable cavity systems can also be used to emulate the dynamics of the classically intractable many-body quantum systems due to their rapidly-growing Hilbert space [12, 13]. Recent success in realization of boson sampling of microwave photons to emulate the optical vibrational spectra of triatomic molecules [14] is an example of an early experimental step towards this goal.

The advantages brought by the flexible Hilbert space structure of cavity resonators are accompanied by crucial challenges to manipulate such systems. General quantum operations across several photon number states require highly nonlinear interactions, which are also crucial for many-body photonic quantum simulations. However, the native nonlinear interactions among photons are often weak and untunable. On the other hand, Hamiltonian engineering utilizes controlled operations to generate tailored evolution to deliver complicated tasks beyond the capacity of native interactions, that can be applied to quantum information processing, quantum sensing, and quantum simulation [15–18]. Inspired by advances in the universal control of cavity modes using an ancilla qubit [19–22], here we develop a general formalism to engineer a photon-number dependent (PND) Hamiltonian for cavities appropriate for cQED devices.

Dispersive model with off-resonant drives— We first consider the simplest model of a dispersively coupled [23] qubit-cavity system described by the Hamiltonian

$$\hat{H}_0 = \hbar\omega_a \hat{a}^\dagger \hat{a} + \hbar\omega_q |e\rangle \langle e| - \hbar\chi \hat{a}^\dagger \hat{a} |e\rangle \langle e|, \quad (1)$$

where ω_a is the frequency of the cavity mode \hat{a} , ω_q is the qubit transition frequency between qubit states $|g\rangle$ and $|e\rangle$, and χ is the dispersive coupling strength. The effective qubit transition frequency is dependent upon the number state of the cavity, $|n\rangle$, with resonant frequencies $\omega_{q,n} = \omega_q - \chi n$. Applying a time-dependent drive $\Omega(t)$ to the qubit,

$$\hat{V}(t) = \hbar\Omega(t)\hat{\sigma}_- + \hbar\Omega^*(t)\hat{\sigma}_+, \quad (2)$$

and working in the number-split regime [24–26] where χ is larger than the transition linewidth of both the qubit and the cavity, one can drive the qubit near selective number-dependent transition frequencies to address individual number states of the cavity. In contrast to the recently demonstrated scheme of imparting selective number-dependent arbitrary phases (SNAP) to photon Fock-states by directly exciting qubit transitions [19, 20], here we work in the large drive detuning regime to engineer a continuous photon-number dependent target Hamiltonian.

Specifically, we consider control drives of the form $\Omega(t) = \sum_{m \in \mathbb{Z}} \Omega_m e^{i(\omega_q - m\chi + \delta_m)t}$. Moving the total Hamiltonian $\hat{H}(t) = \hat{H}_0 + \hat{V}(t)$ to the interaction picture with the unitary transformation $\hat{U} = \exp(i\hat{H}_0 t/\hbar)$, we obtain

$$\hat{V}_I(t) = \sum_m \sum_n \hbar\Omega_m (e^{i((n-m)\chi + \delta_m)t} |n\rangle \langle n| \hat{\sigma}_- + \text{H.c.}). \quad (3)$$

Assuming $\forall m, |\Omega_m| \ll |\delta_m|$, we use time-dependent perturbation theory to find an effective Hamiltonian,

$$\hat{H}_{\text{I,eff}} = - \sum_m \sum_n \frac{\hbar|\Omega_m|^2 |n\rangle \langle n| \hat{\sigma}_z}{(n-m)\chi + \delta_m} + \mathcal{O}(\hat{V}^4), \quad (4)$$

which governs the long time dynamics of the system up to the initial and final kicks [27]. Since we are only driving

the qubit off-resonantly with $\forall m, |\Omega_m| \ll |\delta_m|$, we can assume that it stays in its ground state. Moving back to the original frame, the effective Hamiltonian seen by the photon while the qubit stays in its ground state is

$$\hat{H}_{\text{eff,g}} = \hbar\omega_a \hat{a}^\dagger \hat{a} + \langle g | \hat{H}_{\text{I,eff}} | g \rangle = \hbar\omega_a \hat{a}^\dagger \hat{a} + \hat{H}_E. \quad (5)$$

The off-resonant control drives on the ancilla qubit thus effectively generate a photon-number dependent Hamiltonian $\hat{H}_E = \sum_n \hbar E_n |n\rangle \langle n|$ for the cavity .

Rapidly-oscillating micromotion is predicted by the kick operator [16]. The leading order kick operator is

$$\hat{G}_I^{(1)}(t) = \sum_n \sum_m \frac{\Omega_m |n\rangle \langle n| (\hat{\sigma}_- e^{i((n-m)\chi + \delta_m)t} - \text{H.c.})}{i((n-m)\chi + \delta_m)}. \quad (6)$$

To the first order in \hat{V} , an initial state $|n, g\rangle$ will evolve to $|n, g\rangle + \sum_m \frac{\Omega_m |n\rangle \langle n|}{(n-m)\chi + \delta_m} (e^{-i((n-m)\chi + \delta_m)t} - 1) |n, e\rangle$ at time t , showing an oscillating small population of the qubit excited state component $|n, e\rangle$ with a time-averaged probability $p_{n,e} = \sum_m \left| \frac{\Omega_m}{(n-m)\chi + \delta_m} \right|^2 + \left| \sum_m \frac{\Omega_m}{(n-m)\chi + \delta_m} \right|^2$, where the second term is the contribution from the initial kick at $t = 0$. This excited state component can be viewed as coherent oscillations assuming a closed qubit-cavity system. If one chooses detunings commensurate with the dispersive coupling strength χ , the overall micromotion vanishes at a period $T_M = 2\pi/\text{GCD}(\{\delta_m's, \chi\})$, where $\text{GCD}(\{\delta_m's, \chi\})$ is the greatest common divisor among all the detunings and the dispersive shift, and averages to zero at long-time. For quantum gates implemented by PND Hamiltonian, it is essential to design drives such that $T_G = cT_M$ for some $c \in \mathbb{N}$ in order to achieve maximum gate fidelity. Alternatively, one can relax this constraint on T_G by smoothly turning on and off the drive to remove the effect of the initial and the final kicks [28].

PND Hamiltonian engineering— Given a target Hamiltonian,

$$\hat{H}_T = \sum_n \hbar E_{T,n} |n\rangle \langle n|, \quad (7)$$

one may find appropriate values of Ω_m and δ_m such that $\hat{H}_E = \hat{H}_T$. The solution for Ω_m and δ_m for a given target Hamiltonian (with reasonable strengths $E_{T,n} \ll \chi$) is not unique. Here we suggest a way of designing the drives as described below.

First, we consider a finite set of possible detunings $\delta_m's = \{\pm\chi/2, \pm\chi/4\}$. By selecting detunings commensurate with χ , we can ensure that there are no surprising near-resonant higher-order contributions and also easily determine the periodicity at which the micromotion vanishes, $T_M = 8\pi/\chi$ for the chosen set of $\delta_m's$ (or $T_M = 4\pi/\chi$ if $\delta_m's = \{\pm\chi/2\}$). Those detunings are comparable to χ which allows the largest possible engineered Hamiltonian strength. Second, we assign random

choices of drive detunings from $\delta_m's$ for each number state and find the optimized parameters that generate the target Hamiltonian according to Eq. (4) plus fourth-order perturbation theory terms while minimizing $\sum_n p_{n,e}$, the summation of the average qubit excited state probability due to micromotion. The optimized choice also minimizes the decoherence induced by qubit relaxation, which will be discussed later.

Below we present concrete examples to demonstrate versatile applications of PND, with numerical simulation results shown in Fig. 1 [27]. Assuming a dispersive shift $\chi = 2.56$ MHz, we are able to engineer Hamiltonian strengths up to $E_T/2\pi \approx 50$ kHz with high precision. Even larger strengths $E_T/2\pi \approx 150$ kHz are achievable but are subject to imperfections due to sixth- and higher-order terms in the perturbation theory. This energy scale of the engineered Hamiltonian, $E_T/2\pi \approx 50$ kHz (150 kHz), is much larger than the cavity decoherence [29] and is thus favorable to achieve high fidelity gates or to perform quantum simulation.

(i) *Photon-Photon Interaction*: One direct application for PND Hamiltonian engineering is to create tunable photon-photon nonlinear interactions to emulate dynamics of quantum many-body systems with cavity photons [12, 13]. Such nonlinearities are typically weak in native interactions. For example, one can engineer a purely three-photon interaction for cavity photons by setting

$$\hat{H}_T = \hat{H}_3 = \sum_n \hbar K_3 n(n-1)(n-2) |n\rangle \langle n|. \quad (8)$$

(ii) *Parity-Dependent Energy*: Photon number parity serves as an error-syndrome in various bosonic quantum error correction codes such as cat codes and binomial codes [6, 7]. By engineering a Hamiltonian of the form

$$\hat{H}_T = \hat{H}_P = \sum_n \hbar P (-1)^{n+1} |n\rangle \langle n|, \quad (9)$$

the cavity can distinguish photon number parity by energy, which might allow us to design error-detection or dynamical stabilization of the code states for bosonic quantum error correction [30].

(iii) *Error-Transparent Z-Rotation*: Continuous rotation of the encoded logical qubit around the Z-axis can generate the whole family of phase shift gates R_θ , including $\frac{\pi}{8}$ -gate and Z-gate, which are common elements of single-qubit gates for universal quantum computing [31]. For quantum information encoded in rotational-symmetric bosonic code that can correct up to $d_n - 1$ photon loss errors [9], the logical states are

$$|0_{d_n}\rangle_L \equiv \sum_{k=0}^{\infty} f_{2kd_n} |n = 2kd_n\rangle, \quad (10)$$

$$|1_{d_n}\rangle_L \equiv \sum_{k=0}^{\infty} f_{(2k+1)d_n} |n = (2k+1)d_n\rangle, \quad (11)$$

with code-dependent coefficients f_n 's. Phase shift gates at an angle θ for logical states can be implemented via the cavity Kerr effect $\propto (\hat{a}^\dagger \hat{a})^2$ for the Z-gate $\theta = \frac{\pi}{2}$ [6, 9] or by four-photon interaction $\propto (\hat{a}^\dagger \hat{a})^4$ for the $\frac{\pi}{8}$ -gate $\theta = \frac{\pi}{4}$ [9].

To achieve fault-tolerant quantum computation, one can instead design an error-transparent [32–35] Hamiltonian, that commutes with and is thus uninterrupted by the photon-loss error, to perform continuous logical Z-rotations. By engineering the same positive energy shift $\hbar g_R$ for $|0\rangle_L$ and all of its recoverable error states while engineering an equal but opposite energy shift $-\hbar g_R$ for $|1\rangle_L$ and all of its recoverable error states, the resulting Z-rotation is ‘transparent’ to $d_n - 1$ photon-loss-errors. Specifically, for cat codes or binomial codes with $d_n = 2$,

$$\hat{H}_Z = \sum_{k=0}^{\infty} \hbar g_R (|4k\rangle \langle 4k| + |4k+3\rangle \langle 4k+3| - |4k+2\rangle \langle 4k+2| - |4k+1\rangle \langle 4k+1|). \quad (12)$$

Consider the $\frac{\pi}{8}$ -gate ($\theta = \frac{\pi}{4}$) on the kitten code $|0\rangle_k = \frac{1}{\sqrt{2}}(|0\rangle + |4\rangle)$, $|1\rangle_k = |2\rangle$ [7] for example. This rotation can be implemented by applying \hat{H}_Z for a time $t = \frac{\pi}{8g_R}$, by imparting phase $-\frac{\pi}{8}$ on $|n=0,3,4\rangle$ and phase $+\frac{\pi}{8}$ on $|n=1,2\rangle$ with a SNAP gate, or by applying $H_4 = \hbar K_4 (\hat{a}^\dagger \hat{a})^4$ for a time $t = \frac{\pi}{64K_4}$. We characterize the gate performance in the presence of photon loss by performing the rotation gate on $\frac{1}{\sqrt{2}}(|0\rangle_k + |1\rangle_k) \otimes |g\rangle$ over the same gate time, followed by instantaneous single-photon-loss-error recovery [7, 36] in Fig. 1(d). Comparing the final fidelities, the PND gate and the SNAP gate show much higher resilience to photon-loss-error than H_4 due to their error-transparent structure.

Qubit-induced decoherence— In practice, the decoherence of the qubit may induce cavity dephasing during the PND process. Specifically, the qubit relaxation jump operator $\hat{\sigma}_-$ at a rate $\Gamma_q \ll \chi$ would cause dephasing for off-diagonal density matrix elements of the cavity number states $\rho_{n_1 n_2}$ at a rate $\gamma_{n_1 n_2} = \frac{\Gamma_q}{2}(p_{n_1, e} + p_{n_2, e})$, while the qubit dephasing jump operator $|e\rangle \langle e|$ at a rate $\Gamma_\phi \ll \chi$ causes cavity dephasing at a rate $\gamma_{n_1 n_2} = \frac{\Gamma_\phi}{2}(p_{n_1, e} + p_{n_2, e} - 2 \sum_{m_1} \frac{\Omega_{m_1}^*}{(n_1 - m_1)\chi + \delta_{m_1}} \sum_{m_2} \frac{\Omega_{m_2}}{(n_2 - m_2)\chi + \delta_{m_2}})$. Smoothly turning on the PND drive will remove the contribution to $p_{n, e}$ from the initial kick and further reduce the cavity dephasing [27]. Our choice of the optimized parameters for minimizing the micromotion also minimizes the decoherence induced by qubit relaxation, which is the dominant source of imperfection in typical cQED devices.

In contrast to the resonantly-driven SNAP gate which has an averaged qubit-excited state probability $\frac{1}{2}$ during the operation, our scheme has a suppressed qubit excitation and thus has a much smaller decoherence rate during the operation. At the end of the gate operation, the overall qubit-induced decoherence for the PND gate scales as

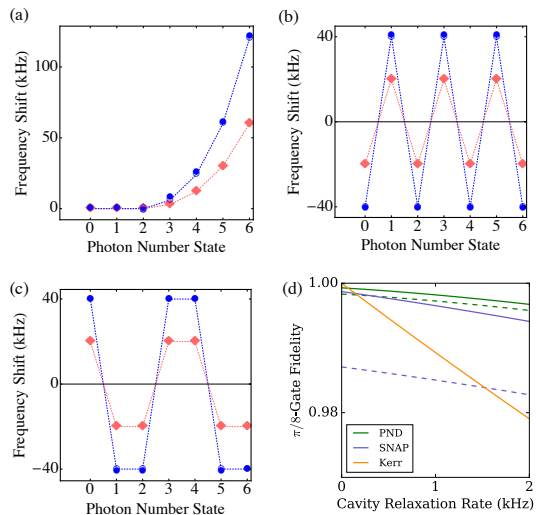


FIG. 1. Simulation of the PND Hamiltonian engineering frequency shifts for (a) three-photon interaction, (b) parity-dependent energy, and (c) error-transparent Z-rotation. The target Hamiltonian ($E_{T,n}/2\pi$) is shown in dotted lines with open markers, the engineered Hamiltonian ($E_n/2\pi$) is represented by solid markers, and different colors represent different engineered Hamiltonian strengths. (d) Fidelity of $\pi/8$ -gate as a function of the cavity relaxation rate. Dashed lines represent the modifications due to ancilla qubit relaxation at a rate $\Gamma_q/2\pi = 3$ kHz. Here we assume $\chi/2\pi = 2.56$ MHz and $\pi/8$ -gate time $T_G = 16\pi/\chi = 2T_M$.

$\frac{\Gamma_q \Omega_n^2 T_G}{2\chi^2} \approx \frac{|\phi_n| \Gamma_q}{2\chi}$, where ϕ_n is the phase imparted on the number state $|n\rangle$, while the qubit-induced overall decoherence for the SNAP gate scales as $\frac{\Gamma_q T_G}{2} = \frac{\pi \Gamma_q}{\Omega}$ regardless of the phase (limited by $|\Omega| \ll \chi$).

The SNAP and PND schemes complement each other for photon-number dependent operations. The SNAP gate is ideal for one-shot operation to impart large phases. On the other hand, the PND Hamiltonian engineering scheme is better suited for quantum simulation, continuous operation, and quantum gate with small phases. In Fig. 1(d) we show the $\frac{\pi}{8}$ -gate fidelity modified by a lossy qubit in dashed lines. The off-resonantly driven PND gate accumulates much less decoherence (qubit-induced infidelity=0.075%) than the SNAP gate (qubit-induced infidelity=0.91%), assuming no cavity relaxation. Since the qubit-induced decoherence for the PND gate is proportional to the imparted phase, the maximal qubit-induced PND R_θ gate infidelity is 0.6% for $\theta = 2\pi$, which suggests that the PND scheme shall outperform the SNAP scheme (with the given gate time) for arbitrary error-transparent R_θ gate.

PND Hamiltonian engineering with Kerr— So far we have been working with the dispersive model of the qubit-cavity coupling. In reality, the underlying microscopic model of coupled qubit-cavity system also predicts higher-order coupling terms [37, 38]. Now consider a gen-

eralized model with photon self-Kerr K and second-order dispersive shift χ' , the Hamiltonian reads

$$\begin{aligned} \hat{H}_0 = & \hbar\omega_a \hat{a}^\dagger \hat{a} + \hbar\omega_q |e\rangle \langle e| - \hbar\chi \hat{a}^\dagger \hat{a} |e\rangle \langle e| - \frac{\hbar K}{2} \hat{a}^\dagger \hat{a}^\dagger \hat{a} \hat{a} \\ & + \frac{\hbar\chi'}{2} \hat{a}^\dagger \hat{a}^\dagger \hat{a} \hat{a} |e\rangle \langle e|. \end{aligned} \quad (13)$$

Adding control drives $\Omega(t) = \sum_m \Omega_m e^{i(\omega_q - m\chi + \delta_m)}$ and assuming $\forall m, |\Omega_m| \ll |\delta_m|$, one can again use time-dependent perturbation theory to find an effective Hamiltonian similar to eq. (4) but with every $n\chi$ replaced by $n\chi - \chi'n(n-1)/2$ due to the second-order dispersive shift [27].

The effective Hamiltonian seen by the photon while the qubit stays in its ground state is

$$H_{\text{eff,g}} = \hbar\omega_a \hat{a}^\dagger \hat{a} - \frac{\hbar K}{2} \hat{a}^\dagger \hat{a}^\dagger \hat{a} \hat{a} + \langle g | H_{1,\text{eff}} | g \rangle. \quad (14)$$

The self-Kerr effect is the leading order correction to cavity resonators that can cause unwanted rotations and (in the presence of photon loss can) introduce extra decoherence. We can apply this Kerr-corrected Hamiltonian engineering scheme to cancel the cavity self-Kerr by choosing $\sum_n \hbar E_{T,n} |n\rangle \langle n| = \frac{\hbar K}{2} \hat{a}^\dagger \hat{a}^\dagger \hat{a} \hat{a}$, or to engineer a target Hamiltonian while canceling Kerr. Numerical simulation of PND Kerr cancellation is presented in Fig. 2. Taking $\chi/2\pi = 2$ MHz, $K/2\pi = 3$ kHz, and assuming no photon loss, one can preserve a cat state with close to unit fidelity for $t = 20\mu\text{s}$ and 99.2 % fidelity for $t = 100\mu\text{s}$ with PND Kerr cancellation [27].

PND Hamiltonian engineering for coupled cavities— Here we further generalize our PND scheme to the case of coupled cavities. Specifically, we consider two cavity modes \hat{a} and \hat{b} dispersively coupled to their own ancilla qubits $\hat{\sigma}^a$, $\hat{\sigma}^b$ and to another joint qubit $\hat{\sigma}^c$ with a dispersive shift χ_c [34], assumed to be equal for both modes,

$$\begin{aligned} \hat{H}_0 = & \hbar\omega_a \hat{a}^\dagger \hat{a} + \hbar\omega_{q,a} |e_a\rangle \langle e_a| - \hbar\chi_a \hat{a}^\dagger \hat{a} |e_a\rangle \langle e_a| \\ & + \hbar\omega_b \hat{b}^\dagger \hat{b} + \hbar\omega_{q,b} |e_b\rangle \langle e_b| - \hbar\chi_b \hat{b}^\dagger \hat{b} |e_b\rangle \langle e_b| \\ & + \hbar\omega_{q,c} |e_c\rangle \langle e_c| - \hbar\chi_c (\hat{a}^\dagger \hat{a} + \hat{b}^\dagger \hat{b}) |e_c\rangle \langle e_c|, \end{aligned} \quad (15)$$

where $\omega_{a/b}$ are the frequencies of the cavities, $\omega_{q,a/b/c}$ are the qubit transition frequencies between $|g_{a/b/c}\rangle$ and $|e_{a/b/c}\rangle$, and $\chi_{a/b/c}$ are the dispersive coupling strengths. One can drive the coupled qubit $\hat{\sigma}^c$ to control cavity states dependent on $n_a + n_b$ and drive qubits $\hat{\sigma}^a$ and $\hat{\sigma}^b$ to control cavity states dependent on n_a and n_b respectively. Altogether, one can engineer a two-cavity Hamiltonian $\hat{H}_E = \sum_{n_a, n_b} \hbar E_{n_a n_b} |n_a n_b\rangle \langle n_a n_b| = \sum_{n_a, n_b} \hbar(E_{c, n_a + n_b} + E_{a, n_a} + E_{b, n_b}) |n_a n_b\rangle \langle n_a n_b|$ [27].

We can apply this generalized PND scheme to implement controlled-Z-rotations for realizing controlled-phase gates CPHASE(θ), which is one class of essential two-qubit entangling gates for universal quantum computing. For bosonic-encoded qubits, the CPHASE gate has been

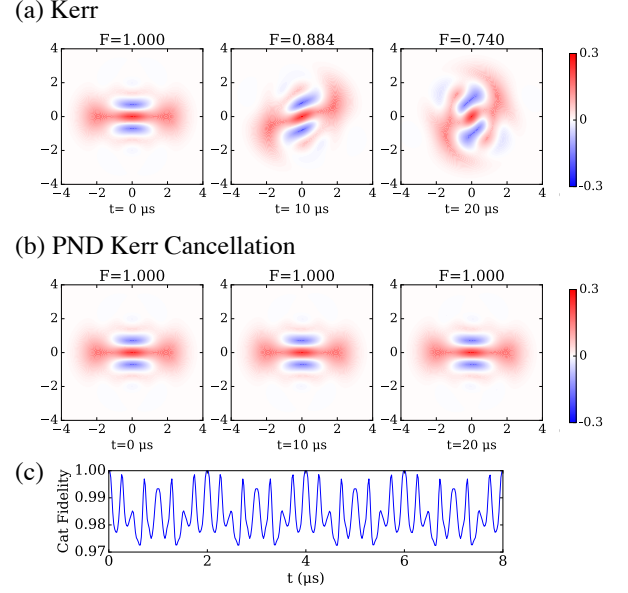


FIG. 2. Simulated evolution of the cavity cat state $\frac{1}{\sqrt{2}}(|\alpha_c\rangle + |-\alpha_c\rangle)$, an even superposition of coherent states with opposite phases. (a) Wigner function snapshots of the cat state evolving under the cavity self-Kerr. (b) Wigner function snapshots of the cat state with PND Kerr cancellation. (c) Cat state fidelity as a function of time under PND Kerr cancellation, showing a clear signature of the micromotion. Here we assume $\alpha_c = \sqrt{2}$, cutoff photon number $N_{\text{cut}} = 6$, $\chi/2\pi = 2$ MHz, $K/2\pi = 3$ kHz, $\chi'/2\pi = 6$ kHz, and $T_M = 2\mu\text{s}$.

demonstrated fairly recently, though in a protocol susceptible to photon loss during the gate operation [39]. Here we present an error-transparent operation [32, 33] of controlled-Z-rotation by PND which is tolerant against photon loss in the cavities.

We design an error-transparent Hamiltonian \hat{H}_{cR} for CPHASE(θ) such that within a total number distance $d_n = \min(d_{n_a}, d_{n_b})$ and its error states have the same negative energy shift $\hbar g_{cR}$,

$$\begin{aligned} \hat{H}_{cR} = & -\hbar g_{cR} \sum_{k=0}^{\infty} \sum_{l_a=0}^{d_n-1} |(2k+1)d_{n_a} - l_a\rangle \langle (2k+1)d_{n_a} - l_a|_a \\ & \otimes \sum_{l_b=0}^{d_n-1-l_a} |(2k+1)d_{n_b} - l_b\rangle \langle (2k+1)d_{n_b} - l_b|_b, \end{aligned} \quad (16)$$

up to residual energy shifts on error states with total photon loss number exceeding $d_n - 1$. The targeted energy shifts to implement \hat{H}_{cR} for $d_n = d_{n_a} = d_{n_b} = 2$ and the numerically simulated engineered energy shifts by the generalized PND are shown in Fig. 3(a). The simulated fidelity of a controlled- $\pi/8$ -gate starting from the kitten-code encoded state $\frac{1}{2}(|0_a\rangle_k + |1_a\rangle_k) \otimes (|0_b\rangle_k + |1_b\rangle_k) \otimes |g_a g_b g_c\rangle$, followed by instantaneous single-photon-

loss recovery in both cavities, is larger than 99.8% even in the presence of the relaxation of all three ancilla qubits (Fig. 3(b)).

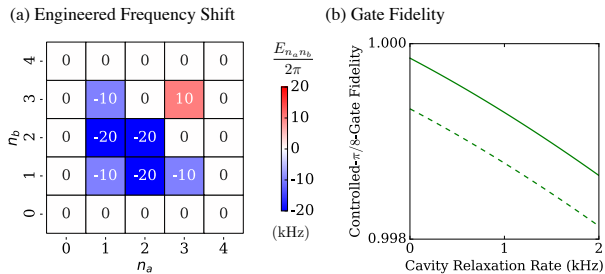


FIG. 3. (a) Simulated engineered energy shifts for error-transparent controlled-rotation as a function of the photon numbers of coupled cavities. (b) Fidelity of PND controlled- $\pi/8$ -gate as a function of the total cavity relaxation rate. The dashed line represents the modifications due to ancilla qubit relaxation at a rate $\Gamma_{qa}/2\pi = \Gamma_{qb}/2\pi = \Gamma_{qc}/2\pi = 3$ kHz. Here we assume $\chi_a/2\pi = \chi_b/2\pi = \chi_c/2\pi = 2.56$ MHz, the controlled- $\pi/8$ -gate time $T_G = 16\pi/\chi = 2T_M$, and that the two cavities have the same relaxation rate.

In conclusion, we have developed a toolbox for photon-number dependent Hamiltonian engineering by off-resonantly driving ancilla qubit(s). We provide a general formalism to design and optimize the control drives for engineering arbitrary single-cavity target Hamiltonian and performing quantum gates, with examples include three-photon interaction, parity-dependent energy, error-transparent Z-rotation for rotation-symmetric bosonic qubits, and cavity self-Kerr cancellation. We can also generalize this scheme to implement error-transparent controlled-rotation between two cavities. The flexible and thus highly nonlinear engineered Hamiltonian for photons admits versatile applications for quantum simulation and quantum information processing. Our scheme can be implemented with dispersively coupled microwave cavities and transmon qubits in the cQED platform. Recent demonstration of the strong dispersive regime in a surface acoustic wave resonator [40, 41] indicates opportunities for phonon-number dependent operations as well.

Looking forward, exploring fault-tolerant approaches such as qubit-error-transparent [34] or path-independent [42, 43] gates may further reduce the decoherence induced by the ancilla qubit. Robust and continuous control of cavities can assist quantum sensing and realize universal fault-tolerant quantum gates with potential compatibility with autonomous quantum error correction [28, 35, 36, 44]. For future prospects of many-body quantum simulation with photons [12], applying our scheme to create local interactions in coupled cavities can offer opportunities for studying exotic phenomena of extended Bose-Hubbard model with three- or more-body interactions [45].

We acknowledge support from the ARL-CDQI (W911NF-15-2-0067), ARO (W911NF-18-1-0020, W911NF-18-1-0212), ARO MURI (W911NF-16-1-0349), AFOSR MURI (FA9550-15-1-0015, FA9550-19-1-0399), DOE (DE-SC0019406), NSF (EFMA-1640959, OMA-1936118), and the Packard Foundation (2013-39273).

* chiao@uchicago.edu

- [1] R. J. Schoelkopf and S. M. Girvin, *Nature (London)* **451**, 664 (2008).
- [2] M. H. Devoret and R. J. Schoelkopf, *Science* **339**, 1169 (2013).
- [3] M. Kjaergaard, M. E. Schwartz, J. Braumüller, P. Krantz, J. I.-J. Wang, S. Gustavsson, and W. D. Oliver, *Annu. Rev. Condens. Matter Phys.* **11** (2019).
- [4] C. U. Lei, L. Krayzman, S. Ganjam, L. Frunzio, and R. J. Schoelkopf, *Appl. Phys. Lett.* **116**, 154002 (2020).
- [5] D. Gottesman, A. Kitaev, and J. Preskill, *Phys. Rev. A* **64**, 123101 (2001).
- [6] M. Mirrahimi, Z. Leghtas, V. V. Albert, S. Touzard, R. J. Schoelkopf, L. Jiang, and M. H. Devoret, *New J. Phys.* **16**, 045014 (2014).
- [7] M. H. Michael, M. Silveri, R. T. Brierley, V. V. Albert, J. Salmilehto, L. Jiang, and S. M. Girvin, *Phys. Rev. X* **6**, 031006 (2016).
- [8] V. V. Albert, K. Noh, K. Duivenvoorden, D. J. Young, R. T. Brierley, P. Reinhold, C. Vuillot, L. Li, C. Shen, S. M. Girvin, B. M. Terhal, and L. Jiang, *Phys. Rev. A* **97**, 032346 (2018).
- [9] A. L. Grimsmo, J. Combes, and B. Q. Baragiola, *Phys. Rev. X* **10**, 011058 (2020).
- [10] A. Grimm, N. E. Frattini, S. Puri, S. O. Mundhada, S. Touzard, M. Mirrahimi, S. M. Girvin, S. Shankar, and M. H. Devoret, *Nature (London)* **584**, 205 (2020).
- [11] N. Ofek, A. Petrenko, R. Heeres, P. Reinhold, Z. Leghtas, B. Vlastakis, Y. Liu, L. Frunzio, S. M. Girvin, L. Jiang, M. Mirrahimi, M. H. Devoret, and R. J. Schoelkopf, *Nature (London)* **536**, 441 (2016).
- [12] M. J. Hartmann, *J. Opt.* **18**, 104005 (2016).
- [13] C. Noh and D. G. Angelakis, *Reports Prog. Phys.* **80**, 016401 (2017).
- [14] C. S. Wang, J. C. Curtis, B. J. Lester, Y. Zhang, Y. Y. Gao, J. Freeze, V. S. Batista, P. H. Vaccaro, I. L. Chuang, L. Frunzio, L. Jiang, S. M. Girvin, and R. J. Schoelkopf, *Phys. Rev. X* **10**, 021060 (2020).
- [15] S. G. Schirmer, *Lect. Notes Control Inf. Sci.* **366 LNCIS**, 293 (2006).
- [16] N. Goldman and J. Dalibard, *Phys. Rev. X* **4**, 031027 (2014).
- [17] P. Krantz, M. Kjaergaard, F. Yan, T. P. Orlando, S. Gustavsson, and W. D. Oliver, *Appl. Phys. Rev.* **6**, 021318 (2019).
- [18] H. Haas, D. Puzzuoli, F. Zhang, and D. G. Cory, *New J. Phys.* **21**, 103011 (2019).
- [19] S. Krastanov, V. V. Albert, C. Shen, C.-L. L. Zou, R. W. Heeres, B. Vlastakis, R. J. Schoelkopf, and L. Jiang, *Phys. Rev. A* **92**, 040303 (2015).
- [20] R. W. Heeres, B. Vlastakis, E. Holland, S. Krastanov, V. V. Albert, L. Frunzio, L. Jiang, and R. J. Schoelkopf, *Phys. Rev. Lett.* **115**, 137002 (2015).

- [21] R. W. Heeres, P. Reinhold, N. Ofek, L. Frunzio, L. Jiang, M. H. Devoret, and R. J. Schoelkopf, *Nat. Commun.* **8**, 1 (2017).
- [22] Y. Y. Gao, B. J. Lester, K. S. Chou, L. Frunzio, M. H. Devoret, L. Jiang, S. M. Girvin, and R. J. Schoelkopf, *Nature (London)* **566**, 509 (2019).
- [23] M. Boissonneault, J. M. Gambetta, and A. Blais, *Phys. Rev. A* **79**, 013819 (2009).
- [24] J. Gambetta, A. Blais, D. I. Schuster, A. Wallraff, L. Frunzio, J. Majer, M. H. Devoret, S. M. Girvin, and R. J. Schoelkopf, *Phys. Rev. A* **74**, 042318 (2006).
- [25] D. I. Schuster, A. A. Houck, J. A. Schreier, A. Wallraff, J. M. Gambetta, A. Blais, L. Frunzio, J. Majer, B. Johnson, M. H. Devoret, S. M. Girvin, and R. J. Schoelkopf, *Nature (London)* **445**, 515 (2007).
- [26] B. R. Johnson, M. D. Reed, A. A. Houck, D. I. Schuster, L. S. Bishop, E. Ginossar, J. M. Gambetta, L. Dicarlo, L. Frunzio, S. M. Girvin, and R. J. Schoelkopf, *Nat. Phys.* **6**, 663 (2010).
- [27] See Supplemental Material at [URL].
- [28] Throughout the maintext we assume the drive is abruptly turned on at $t = 0$. Please refer to the Supplemental Material for details on smooth ramping of the drive.
- [29] M. Reagor, H. Paik, G. Catelani, L. Sun, C. Axline, E. Holland, I. M. Pop, N. A. Masluk, T. Brecht, L. Frunzio, M. H. Devoret, L. Glazman, and R. J. Schoelkopf, *Appl. Phys. Lett.* **102**, 192604 (2013).
- [30] José Lebreuilly, Kyungjoo Noh, Chiao-Hsuan Wang, S. M. Girvin, and Liang Jiang, in preparation.
- [31] M. A. Nielsen and I. Chuang, *Quantum Computation and Quantum Information: 10th Anniversary Edition* (Cambridge University Press, Cambridge, UK, 2010).
- [32] O. Vy, X. Wang, and K. Jacobs, *New J. Phys.* **15**, 053002 (2013).
- [33] E. Kapit, *Phys. Rev. Lett.* **120**, 050503 (2018).
- [34] S. Rosenblum, P. Reinhold, M. Mirrahimi, L. Jiang, L. Frunzio, and R. J. Schoelkopf, *Science* **361**, 266 (2018).
- [35] Y. Ma, Y. Xu, X. Mu, W. Cai, L. Hu, W. Wang, X. Pan, H. Wang, Y. P. Song, C. L. Zou, and L. Sun, *Nat. Phys.* **16**, 827 (2020).
- [36] J. M. Lihm, K. Noh, and U. R. Fischer, *Phys. Rev. A* **98**, 12317 (2018).
- [37] J. Koch, T. M. Yu, J. Gambetta, A. A. Houck, D. I. Schuster, J. Majer, A. Blais, M. H. Devoret, S. M. Girvin, and R. J. Schoelkopf, *Phys. Rev. A* **76**, 042319 (2007).
- [38] G. Kirchmair, B. Vlastakis, Z. Leghtas, S. E. Nigg, H. Paik, E. Ginossar, M. Mirrahimi, L. Frunzio, S. M. Girvin, and R. J. Schoelkopf, *Nature (London)* **495**, 205 (2013).
- [39] Y. Xu, Y. Ma, W. Cai, X. Mu, W. Dai, W. Wang, L. Hu, X. Li, J. Han, H. Wang, Y. P. Song, Z. B. Yang, S. B. Zheng, and L. Sun, *Phys. Rev. Lett.* **124**, 120501 (2020).
- [40] L. R. Sletten, B. A. Moores, J. J. Viennot, and K. W. Lehnert, *Phys. Rev. X* **9**, 021056 (2019).
- [41] P. Arrangoiz-Arriola, E. A. Wollack, Z. Wang, M. Pechal, W. Jiang, T. P. McKenna, J. D. Witmer, R. Van Laer, and A. H. Safavi-Naeini, *Nature (London)* **571**, 537 (2019).
- [42] P. Reinhold, S. Rosenblum, W. L. Ma, L. Frunzio, L. Jiang, and R. J. Schoelkopf, *Nat. Phys.* **16**, 822 (2020).
- [43] W.-L. Ma, M. Zhang, Y. Wong, K. Noh, S. Rosenblum, P. Reinhold, R. J. Schoelkopf, and L. Jiang, (2020), [arXiv:1911.12240v2](https://arxiv.org/abs/1911.12240v2).
- [44] E. Kapit, *Phys. Rev. Lett.* **116**, 150501 (2016).
- [45] O. Dutta, M. Gajda, P. Hauke, M. Lewenstein, D.-S. Lühmann, B. A. Malomed, T. Sowiński, and J. Zakrzewski, *Reports Prog. Phys.* **78**, 066001 (2015).

Supplemental Information for "Photon-Number Dependent Hamiltonian Engineering for Cavities"

Chiao-Hsuan Wang, Kyungjoo Noh, José Lebreuilly, S. M. Girvin, and Liang Jiang

I. DISPERSIVE MODEL

A. Unitary Evolution

Here we calculate the perturbative expansion of the unitary evolution operator for an off-resonantly driven, dispersively coupled qubit-oscillator system described by the Hamiltonian [1]

$$\hat{H}(t) = \hbar\omega_a \hat{a}^\dagger \hat{a} + \hbar\omega_q |e\rangle \langle e| - \hbar\chi \hat{a}^\dagger \hat{a} |e\rangle \langle e| + \hbar\Omega(t) \hat{\sigma}_- + \hbar\Omega^*(t) \hat{\sigma}_+ \equiv \hat{H}_0 + \hat{V}(t), \quad (\text{S1})$$

where $\hat{V}(t) = \hbar\Omega(t) \hat{\sigma}_- + \hbar\Omega^*(t) \hat{\sigma}_+$ with $\Omega(t) = \sum_m \Omega_m e^{i(\omega_q - m\chi + \delta_m)t}$. We assume a tripartition ansatz for the evolution operator $\hat{U}_S(t_f, t_i)$ such that $|\psi(t_f)\rangle \equiv \hat{U}_S(t_f, t_i) |\psi(t_i)\rangle$ for an initial state $|\psi(t_i)\rangle$ and a final state $|\psi(t_f)\rangle$ [2],

$$\hat{U}_S(t_f, t_i) = e^{-i\hat{G}(t_f)} e^{-i\hat{H}_{\text{eff}}(t_f - t_i)/\hbar} e^{i\hat{G}(t_i)}, \quad (\text{S2})$$

where the evolution is separated into a time-independent effective Hamiltonian \hat{H}_{eff} governing the long-time dynamics, as well as initial and final kicks, $\hat{G}(t_i)$ and $\hat{G}(t_f)$. The subscript S denotes evolution in the Schrödinger picture.

Move to the interaction picture with the unitary transformation $\hat{U} = \exp(i\hat{H}_0 t/\hbar)$, we are left with the term

$$\hat{V}_I(t) = \hat{U} \hat{H} \hat{U}^\dagger - i\hbar \hat{U} \hat{U}^\dagger = \sum_m \sum_n \hbar(\Omega_m e^{i((n-m)\chi + \delta_m)t} |n\rangle \langle n| \hat{\sigma}_- + H.c.). \quad (\text{S3})$$

Here the subscript I denotes operators in the interaction picture, $\hat{O}_I(t) = e^{i\hat{H}_0 t/\hbar} \hat{O}(t) e^{-i\hat{H}_0 t/\hbar}$. The evolution operator in the interaction picture is connected to the Schrödinger picture one by

$$\hat{U}_I(t_f, t_i) = e^{i\hat{H}_0 t_f/\hbar} e^{-i\hat{G}(t_f)} e^{-i\hat{H}_{\text{eff}}(t_f - t_i)/\hbar} e^{i\hat{G}(t_i)} e^{-i\hat{H}_0 t_i/\hbar} = e^{-i\hat{G}_I(t_f)} e^{-i(\hat{H}_{\text{eff}} - \hat{H}_0)(t_f - t_i)/\hbar} e^{i\hat{G}_I(t_i)}. \quad (\text{S4})$$

Assuming $|\Omega_m| \ll \chi, |\delta_m|$, we can use time-dependent perturbation theory to calculate $\hat{U}_I(t_f, t_i)$ in powers of \hat{V}_I and find the perturbative expansion of \hat{H}_{eff} and $\hat{G}_I(t)$ such that $\hat{H}_{\text{eff}} = \hat{H}_{\text{eff}}^{(0)} + \hat{H}_{\text{eff}}^{(1)} + \hat{H}_{\text{eff}}^{(2)} + \dots$ and $\hat{G}_I(t) = \hat{G}_I^{(0)}(t) + \hat{G}_I^{(1)}(t) + \hat{G}_I^{(2)}(t) + \dots$.

Specifically,

$$\hat{U}_I(t_f, t_i) = 1 - \frac{i}{\hbar} \int_{t_i}^{t_f} \hat{V}_I(t_1) dt_1 + \left(\frac{-i}{\hbar}\right)^2 \int_{t_i}^{t_f} dt_1 \int_{t_i}^{t_1} dt_2 \hat{V}_I(t_1) \hat{V}_I(t_2) + \dots \quad (\text{S5})$$

For the zeroth order, we have $\hat{G}_I^{(0)}(t) = 0$ and $\hat{H}_{\text{eff}}^{(0)} - \hat{H}_0 = 0$. For $\mathcal{O}(\hat{V})$,

$$-\frac{i}{\hbar} \int_{t_i}^{t_f} \hat{V}_I(t_1) dt_1 = -i\hat{G}_I^{(1)}(t_f) - \frac{i}{\hbar} \hat{H}_{\text{eff}}^{(1)}(t_f - t_i) + i\hat{G}_I^{(1)}(t_i). \quad (\text{S6})$$

We find

$$-\langle n, g | \frac{i}{\hbar} \int_{t_i}^{t_f} \hat{V}_I(t_1) dt_1 | n, g \rangle = -\langle n, e | \frac{i}{\hbar} \int_{t_i}^{t_f} \hat{V}_I(t_1) dt_1 | n, e \rangle = 0, \quad (\text{S7})$$

and

$$-\langle n, g | \frac{i}{\hbar} \int_{t_i}^{t_f} \hat{V}_I(t_1) dt_1 | n, e \rangle = -i \sum_m \frac{\Omega_m e^{i((n-m)\chi + \delta_m)t_f} - \Omega_m e^{i((n-m)\chi + \delta_m)t_i}}{i((n-m)\chi + \delta_m)}. \quad (\text{S8})$$

Thus, we have

$$\hat{H}_{\text{eff}}^{(1)} = 0, \quad (\text{S9})$$

$$\hat{G}_I^{(1)}(t) = \sum_m \sum_n \frac{|n\rangle \langle n|}{i((n-m)\chi + \delta_m)} (\Omega_m \hat{\sigma}_- e^{i((n-m)\chi + \delta_m)t} - \Omega_m^* \hat{\sigma}_+ e^{-i((n-m)\chi + \delta_m)t}). \quad (\text{S10})$$

For $\mathcal{O}(\hat{V}^2)$,

$$\begin{aligned} \left(\frac{-i}{\hbar}\right)^2 \int_{t_i}^{t_f} dt_1 \int_{t_i}^{t_1} dt_2 \hat{V}_I(t_1) \hat{V}_I(t_2) &= -i \hat{G}_I^{(2)}(t_f) - \frac{i}{\hbar} \hat{H}_{\text{eff}}^{(2)}(t_f - t_i) + i \hat{G}_I^{(2)}(t_i) + \frac{1}{2} \left(\frac{-i \hat{H}_{\text{eff}}^{(1)}(t_f - t_i)}{\hbar}\right)^2 \\ + \frac{1}{\hbar} \hat{H}_{\text{eff}}^{(1)}(t_f - t_i) \hat{G}_I^{(1)}(t_i) - \frac{1}{\hbar} \hat{G}_I^{(1)}(t_f) \hat{H}_{\text{eff}}^{(1)}(t_f - t_i) &+ \hat{G}_I^{(1)}(t_f) \hat{G}_I^{(1)}(t_i) - \frac{\hat{G}_I^{(1)}(t_i)^2}{2} - \frac{\hat{G}_I^{(1)}(t_f)^2}{2}. \end{aligned} \quad (\text{S11})$$

We find

$$\hat{H}_{\text{eff}}^{(2)} = - \sum_m \sum_n \frac{\hbar |\Omega_m|^2 |n\rangle \langle n|}{(n-m)\chi + \delta_m} \hat{\sigma}_z, \quad (\text{S12})$$

$$\hat{G}_I^{(2)}(t) = - \sum_{m_1} \sum_{m_2 \neq m_1} \sum_n \frac{\Omega_{m_1} \Omega_{m_2}^* e^{i(\delta_{m_1} - \delta_{m_2} - (m_1 - m_2)\chi)t} - \Omega_{m_1}^* \Omega_{m_2} e^{-i(\delta_{m_1} - \delta_{m_2} - (m_1 - m_2)\chi)t}}{2i((n-m_1)\chi + \delta_{m_1})(\delta_{m_1} - \delta_{m_2} - (m_1 - m_2)\chi)} |n\rangle \langle n| \hat{\sigma}_z. \quad (\text{S13})$$

The third- and fourth-order terms in the effective Hamiltonian are

$$\hat{H}_{\text{eff}}^{(3)} = 0, \quad (\text{S14})$$

$$\begin{aligned} \hat{H}_{\text{eff}}^{(4)} &= \sum_{m_1} \sum_{m_2} \sum_n \frac{\hbar |\Omega_{m_1}|^2 |\Omega_{m_2}|^2 |n\rangle \langle n| \hat{\sigma}_z}{((n-m_1)\chi + \delta_{m_1})((n-m_2)\chi + \delta_{m_2})^2} \\ &- \sum_{m_1} \sum_{m_2 \neq m_1} \sum_n \frac{\hbar |\Omega_{m_1}|^2 |\Omega_{m_2}|^2 |n\rangle \langle n| \hat{\sigma}_z}{((n-m_1)\chi + \delta_{m_1})^2 (\delta_{m_1} - \delta_{m_2} - (m_1 - m_2)\chi)} \\ &+ \sum_{m_1, m_2, m_3, m_4} \sum_n \frac{\hbar \Omega_{m_1} \Omega_{m_2}^* \Omega_{m_3} \Omega_{m_4}^* |n\rangle \langle n| \hat{\sigma}_z}{((n-m_4)\chi + \delta_{m_4})(\delta_{m_1} - \delta_{m_2} - (m_1 - m_2)\chi)((n-m_1)\chi + \delta_{m_1})}, \end{aligned} \quad (\text{S15})$$

where the last term satisfies the condition $\delta_{m_1} - m_1\chi + \delta_{m_3} - m_3\chi = \delta_{m_2} - m_2\chi + \delta_{m_4} - m_4\chi$, and $m_1 \neq m_2 \neq m_3 \neq m_4$ or $m_1 = m_3 \neq m_2 \neq m_4$ or $m_2 = m_4 \neq m_1 \neq m_3$.

Consider special cases where δ_m are commensurable with χ , this problem reduces to a Floquet Hamiltonian with a single periodicity, and one can calculate the Floquet effective Hamiltonian and the kick operator [3] and obtain identical results.

B. Unitary Evolution with Smooth Ramping

So far we have assumed that the drive is abruptly turned on at an initial time t_i and lasts till a final time t_f . One can alternatively apply a ramping function $\lambda(t)$ such that $\hat{H}(t) = \hat{H}_0 + \lambda(t)\hat{V}(t)$ to smoothly turn on (and off) the drive, which will remove the effect associated with the initial (and the final) kick operator if the ramping time scale is much longer than $1/\chi$. The choice of the ramping function $\lambda(t)$ is not unique.

For mathematical simplicity, we first consider the case of applying a sinusoidal envelope $\lambda(t) = \sin(\gamma t)$ to a short-time gate operation from $t = 0$ to $t = T_G = \pi/\gamma$. Using the time-dependent perturbation theory, we find

$$\begin{aligned} & -\frac{i}{\hbar} \int_0^{T_G} \sin(\gamma t_1) \hat{V}_I(t_1) dt_1 \\ &= -\sum_n |n\rangle \langle n| \sum_m \left[\frac{\Omega_m e^{i((n-m)\chi + \delta_m + \gamma)t_1} \hat{\sigma}_-}{2i((n-m)\chi + \delta_m - \gamma)} - \frac{\Omega_m e^{i((n-m)\chi + \delta_m - \gamma)t_1} \hat{\sigma}_-}{2i((n-m)\chi + \delta_m - \gamma)} \right]_0^{\frac{\pi}{\gamma}} + \text{H.c.} \xrightarrow{\chi \gg \gamma} 0, \end{aligned} \quad (\text{S16})$$

and

$$\left(\frac{-i}{\hbar}\right)^2 \int_0^{T_G} dt_1 \int_0^{t_1} dt_2 \sin(\gamma t_1) \hat{V}_I(t_1) \sin(\gamma t_2) \hat{V}_I(t_2) \xrightarrow{\chi \gg \gamma} \sum_m \sum_n \frac{i|\Omega_m|^2 |n\rangle \langle n|}{2((n-m)\chi + \delta_m)} \hat{\sigma}_z. \quad (\text{S17})$$

In the limit $\chi \gg \gamma$, the resulting time evolution with this smooth sinusoidal envelope is thus equivalent to having an effective Hamiltonian generated by $\frac{\hat{V}(t)}{\sqrt{2}}$ but without any initial or final kick effects. To compensate for the $\frac{1}{\sqrt{2}}$ factor, one can implement the same gate (by accumulating the same phase) as the abrupt version $\hat{H}(t) = \hat{H}_0 + \hat{V}(t)$ by rescaling the ramping function to $\lambda_{\text{gate}}(t) = \sqrt{2} \sin(\gamma t)$ or by letting the system evolve twice as long. Note that in the abrupt version one has to choose a gate time at which the micromotion vanishes, while with the sinusoidal envelope there is no such requirement because the micromotion has already been removed by the smooth ramping.

For long-time operation of the PND Hamiltonian engineering scheme, one can design a ramp-up function $\lambda_{\text{up}}(t) = 0 \rightarrow 1$ and a ramp-down function $\lambda_{\text{down}}(t) = 1 \rightarrow 0$ at the beginning and the end of the drive. Here we provide one example of the ramp-up and ramp-down functions,

$$\lambda_{\text{up}}(t) = \begin{cases} \lambda_s \sin[\pi(t - t_i)/2T_s] & t_i \leq t \leq t_i + T_s \\ \frac{\lambda_s - 1}{2} \sin[\pi(t - t_i)/2T_s] + \frac{\lambda_s + 1}{2} & t_i + T_s \leq t \leq t_i + 3T_s \end{cases}, \quad (\text{S18})$$

$$\lambda_{\text{down}}(t) = \begin{cases} \frac{\lambda_s - 1}{2} \sin[\pi(t_f - t)/2T_s] + \frac{\lambda_s + 1}{2} & t_f - 3T_s \leq t \leq t_f - T_s \\ \lambda_s \sin[\pi(t_f - t)/2T_s] & t_f - T_s \leq t \leq t_f \end{cases}, \quad (\text{S19})$$

and $\lambda(t) = 1$ otherwise. Here $\lambda_s = \frac{\sqrt{46}-1}{5}$ is a special chosen value to guarantee the same accumulated phase as the abrupt case during the ramp-up and ramp-down periods.

C. Evolution with Qubit-Induced Dephasing

Here we consider how errors in the ancilla qubit propagates to the cavity mode under off-resonant drives. The ancilla errors are described by the qubit relaxation jump operator $\sqrt{\Gamma_q}\hat{\sigma}_-$ and the qubit dephasing jump operator $\sqrt{\Gamma_\phi}|e\rangle\langle e|$ in the time-dependent Lindblad master equation

$$\partial_t \rho_{tot}(t) = -\frac{i}{\hbar}[H(t), \rho_{tot}(t)] + \mathcal{D}(\rho_{tot}(t)), \quad (\text{S20})$$

where ρ_{tot} is the total density matrix of the coupled qubit-oscillator system, and

$$\begin{aligned} \mathcal{D}(\rho(t)) &= \sum_k \left[J_k \rho(t) J_k^\dagger - \frac{1}{2} J_k^\dagger J_k \rho(t) - \rho(t) \frac{1}{2} J_k^\dagger J_k \right], \\ \{J_k\} &= \{\sqrt{\Gamma_q}\hat{\sigma}_-, \sqrt{\Gamma_\phi}|e\rangle\langle e|\}. \end{aligned} \quad (\text{S21})$$

Moving to the interaction picture, $\hat{\sigma}_-$ becomes $\hat{\sigma}_{-I}(t) = \sum_n |n\rangle\langle n| e^{-i(\omega_q - n\chi)t} \hat{\sigma}_-$ while $|e\rangle\langle e|$ stays the same. Under the rotating wave approximation, when $\Gamma_q \ll \chi$ such that qubit decay will release a photon-number-dependent $\hbar(\omega_q - n\chi)$, we treat the relaxation jump operator as a set of independent jump operators in the cavity number state manifold,

$$\partial_t \rho_{tot,I}(t) = -\frac{i}{\hbar}[V_I(t), \rho_{tot,I}(t)] + \mathcal{D}_I(\rho_{tot,I}(t)). \quad (\text{S22})$$

$$\begin{aligned} \mathcal{D}_I(\rho(t)) &= \sum_k \left[J_{k,I} \rho(t) J_{k,I}^\dagger - \frac{1}{2} J_{k,I}^\dagger J_{k,I} \rho(t) - \rho(t) \frac{1}{2} J_{k,I}^\dagger J_{k,I} \right], \\ \{J_{k,I}\} &= \{\sqrt{\Gamma_\phi}|e\rangle\langle e|, \sqrt{\Gamma_q}\hat{\sigma}_{-}|n\rangle\langle n| \forall n\}. \end{aligned} \quad (\text{S23})$$

We now assume again a tri-partition ansatz for the evolution superoperator $\Lambda_{t_f, t_i}, \rho_I(t_f) \equiv \Lambda_{t_f, t_i} \rho_I(t_i)$,

$$\Lambda_{t_f, t_i} = e^{-\Phi_{t_f}} e^{\tilde{\mathcal{L}}(t_f - t_i)} e^{\Phi_{t_i}}, \quad (\text{S24})$$

such that there is a time-independent Liouvillian $\tilde{\mathcal{L}}$ and a kick superoperator Φ_t that absorbs the time dependence. For $\Gamma_\phi, \Gamma_q, |\Omega_m| \ll \chi$ and $\delta_m \sim \mathcal{O}(\chi)$, one can expand $\tilde{\mathcal{L}}$ and Φ_t in perturbative orders of $\mathcal{O}(\Omega_m, \Gamma_\phi, \Gamma_q)$.

We find the time-independent evolution superoperator as $\tilde{\mathcal{L}} \approx \tilde{\mathcal{L}}^{(1)} + \tilde{\mathcal{L}}^{(2)} + \tilde{\mathcal{L}}^{(3)}$ with

$$\tilde{\mathcal{L}}^{(1)}(\cdot) = \mathcal{D}_I(\cdot), \quad (\text{S25})$$

$$\tilde{\mathcal{L}}^{(2)}(\cdot) = -\frac{i}{\hbar} \left[\hat{H}_{\text{eff}}^{(2)}, \cdot \right], \quad (\text{S26})$$

$$\tilde{\mathcal{L}}^{(3)}(\cdot) = \frac{1}{2} \sum_n \sum_m \frac{1}{((n-m)\chi + \delta_m)^2} ([[\mathcal{S}_-, \mathcal{D}_I], \mathcal{S}_+] + [[\mathcal{S}_+, \mathcal{D}_I], \mathcal{S}_-]) (\cdot), \quad (\text{S27})$$

where $\mathcal{S}_-(\cdot) = [|n\rangle\langle n| \Omega_m \hat{\sigma}_- e^{i((n-m)\chi + \delta_m)t}, \cdot]$, and $\mathcal{S}_+(\cdot) = [|n\rangle\langle n| \Omega_m^* \hat{\sigma}_+ e^{-i((n-m)\chi + \delta_m)t}, \cdot]$, and the kick superoperator as $\Phi_t \approx \Phi_t^{(1)} + \Phi_t^{(2)}$ with

$$\Phi_t^{(1)}(\cdot) = \left[i\hat{G}_I^{(1)}(t), \cdot \right], \quad (\text{S28})$$

$$\Phi_t^{(2)}(\cdot) = \left[i\hat{G}_I^{(2)}(t), \cdot \right] - \sum_n \sum_m \frac{1}{((n-m)\chi + \delta_m)^2} [\mathcal{S}_+ + \mathcal{S}_-, \mathcal{D}_I](\cdot). \quad (\text{S29})$$

Choosing δ_m commensurable with χ such that all the time-dependent terms have a common periodicity T_M , then for $t_f = t_i + cT_M$ for some integer c , $\rho_I(t_i + cT_M) = e^{-\Phi_{t_i}} e^{\tilde{\mathcal{L}}cT_M} e^{\Phi_{t_i}} = e^{\mathcal{L}_F(t_i)cT_M}$ for an Floquet generator $\mathcal{L}_F(t_i) = e^{-\Phi_{t_i}} \tilde{\mathcal{L}} e^{\Phi_{t_i}}$ [4, 5]. Taking $t_i = 0$ and tracing over the ancilla qubit degree of freedom assuming $\rho_{gg} = 1$ and $\rho_{ee} = \rho_{ge} = \rho_{eg} = 0$, then the cavity density matrix in the interaction picture $\rho_{c,I}$ follows a Floquet effective master equation

$$\partial_t \rho_{c,I}(t) \approx -i \left[\sum_m \sum_n \frac{|\Omega_m|^2 |n\rangle \langle n|}{(n-m)\chi + \delta_m}, \rho_{c,I}(t) \right] + \mathcal{D}_{c,I}(\rho_{c,I}(t)), \quad (\text{S30})$$

with jump operators

$$\begin{aligned} \{J_{c,k,I}\} = & \left\{ \frac{\sqrt{\Gamma_\phi} \Omega_m^* |n\rangle \langle n|}{(n-m)\chi + \delta_m}, \frac{\sqrt{\Gamma_q} \Omega_m^* |n\rangle \langle n|}{(n-m)\chi + \delta_m} \middle| \forall n, m \right\} \\ & \cup \left\{ \sum_n \sum_m \frac{\sqrt{\Gamma_\phi} \Omega_m^* |n\rangle \langle n|}{(n-m)\chi + \delta_m} \right\} \cup \left\{ \sum_m \frac{\sqrt{\Gamma_q} \Omega_m^* |n\rangle \langle n|}{(n-m)\chi + \delta_m} \middle| \forall n \right\}. \end{aligned} \quad (\text{S31})$$

The jump operators cause dephasing for off-diagonal density matrix elements of the cavity number states $\rho_{n_1 n_2}$ at a rate

$$\gamma_{n_1 n_2} = \frac{\Gamma_\phi + \Gamma_q}{2} (p_{n_1, e} + p_{n_2, e}) - \Gamma_\phi \sum_{m_1} \frac{\Omega_{m_1}^*}{(n_1 - m_1)\chi + \delta_{m_1}} \sum_{m_2} \frac{\Omega_{m_2}}{(n_2 - m_2)\chi + \delta_{m_2}}, \quad (\text{S32})$$

where $p_{n,e} \equiv \sum_m \left| \frac{\Omega_m}{(n-m)\chi + \delta_m} \right|^2 + \left| \sum_m \frac{\Omega_m}{(n-m)\chi + \delta_m} \right|^2$ is the time-averaged probability of the qubit excited state component $|n, e\rangle$ due to $\hat{G}_I^{(1)}(t)$. The second term in $p_{n,e}$, $\left| \sum_m \frac{\Omega_m}{(n-m)\chi + \delta_m} \right|^2$, is the contribution from the initial kick. Smoothly ramping up the drive can thus reduce the qubit-induced dephasing by removing the effect of the kick.

D. Optimized PND Parameters and additional simulations

In this subsection we show tables of optimized photon-number-dependent (PND) Hamiltonian engineering parameters that minimizes $\sum_n p_{n,e}$. All the engineered frequency shifts are subject to a Fourier transformation precision of ± 0.5 kHz. Here we show optimized parameters with real Ω_m 's. We can also relax the condition and solve for complex values of Ω_m 's, which give rise to similar performance.

Additional simulations for PND error-transparent Z-rotation is shown in Fig. S1 and S2. In Fig. S1 we compare the $\pi/8$ -gate operation via the abrupt PND drive versus the smooth PND drive and find that the smooth ramping scheme reduces the qubit-induced dephasing. In Fig. S2, we study the qubit-induced infidelity for R_θ gate implemented by smooth PND drives. The qubit-induced gate infidelity is proportional to the rotation angle θ (and thus the total phase) while relatively independent of the gate time while θ is fixed, as predicted.

TABLE S1. Three-Photon Interaction: $\chi/2\pi = 2.56$ MHz, $K_3/2\pi = 0.5$ kHz (maintext FIG.1(a) red)

photon number	n=0	n=1	n=2	n=3	n=4	n=5	n=6
target $E_{T,n}/2\pi$ (kHz)	0	0	0	3	12	30	60
engineered $E_n/2\pi$ (kHz)	0	0	0	3	12	30	60
δ_n/χ	1/2	1/2	1/2	1/2	1/2	1/4	1/2
Ω_n/χ	0.0946	0.0694	0.0637	0.0640	0.0661	0.0704	0.0859

TABLE S2. Three-Photon Interaction: $\chi/2\pi = 2.56$ MHz, $K_3/2\pi = 1$ kHz (maintext FIG.1(a) blue)

photon number	n=0	n=1	n=2	n=3	n=4	n=5	n=6
target $E_{T,n}/2\pi$ (kHz)	0	0	0	6	24	60	120
engineered $E_n/2\pi$ (kHz)	0	0	-1	8	25	61	122
δ_n/χ	1/2	1/2	1/2	1/2	1/4	1/2	1/2
Ω_n/χ	0.1422	0.1025	0.0935	0.0917	0.0995	0.1337	0.1172

TABLE S3. Parity-Dependent Energy: $\chi/2\pi = 2.56$ MHz, $P = 20$ kHz (maintext FIG.1(b) red)

photon number	n=0	n=1	n=2	n=3	n=4	n=5	n=6
target $E_{T,n}/2\pi$ (kHz)	-20	20	-20	20	-20	20	-20
engineered $E_n/2\pi$ (kHz)	-20	20	-20	20	-20	20	-20
δ_n/χ	-1/4	1/4	-1/2	1/4	-1/4	1/4	-1/2
Ω_n/χ	0.00682	0.0568	0.0553	0.0349	0.0427	0.0427	0.0786

TABLE S4. Parity-Dependent Energy: $\chi/2\pi = 2.56$ MHz, $P = 40$ kHz (maintext FIG.1(b) blue)

photon number	n=0	n=1	n=2	n=3	n=4	n=5	n=6
target $E_{T,n}/2\pi$ (kHz)	-40	40	-40	40	-40	40	-40
engineered $E_n/2\pi$ (kHz)	-40.5	40.5	-40.5	40.5	-40.5	40.5	-40.5
δ_n/χ	-1/2	1/4	-1/2	1/4	-1/4	1/2	-1/4
Ω_n/χ	0.0232	0.0799	0.0826	0.0463	0.0469	0.0820	0.0816

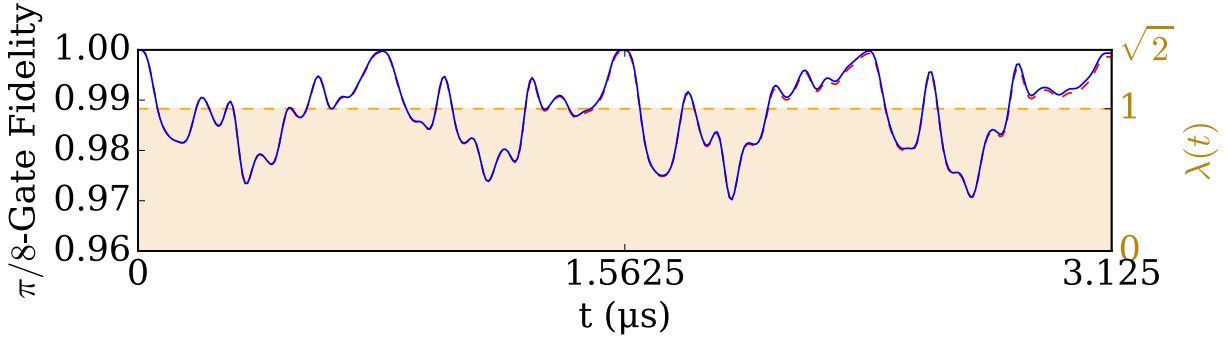
TABLE S5. Error-Transparent Z-rotation: $\chi/2\pi = 2.56$ MHz, $g_R/2\pi = 20$ kHz, $d_n=2$ (maintext FIG.1(c) red, FIG.1(d))

photon number	n=0	n=1	n=2	n=3	n=4	n=5	n=6
target $E_{T,n}/2\pi$ (kHz)	20	-20	-20	20	20	-20	-20
engineered $E_n/2\pi$ (kHz)	20	-20	-20	20	20	-20	-20
δ_n/χ	1/2	-1/2	-1/2	1/4	1/2	-1/4	-1/2
Ω_n/χ	0.0862	0.0531	0.0753	0.0240	0.0554	0.0489	0.0893

TABLE S6. Error-Transparent Z-rotation: $\chi/2\pi = 2.56$ MHz, $g_R/2\pi = 40$ kHz, $d_n=2$ (maintext FIG.1(c) blue)

photon number	n=0	n=1	n=2	n=3	n=4	n=5	n=6
target $E_{T,n}/2\pi$ (kHz)	40	-40	-40	40	40	-40	-40
engineered $E_n/2\pi$ (kHz)	40	-41	-41	40	40	-41	-40
δ_n/χ	1/2	-1/4	-1/2	1/4	1/4	-1/4	-1/2
Ω_n/χ	0.1166	0.0600	-0.0961	0.0308	0.0629	0.0678	0.1214

(a) abrupt drive



(b) smooth drive

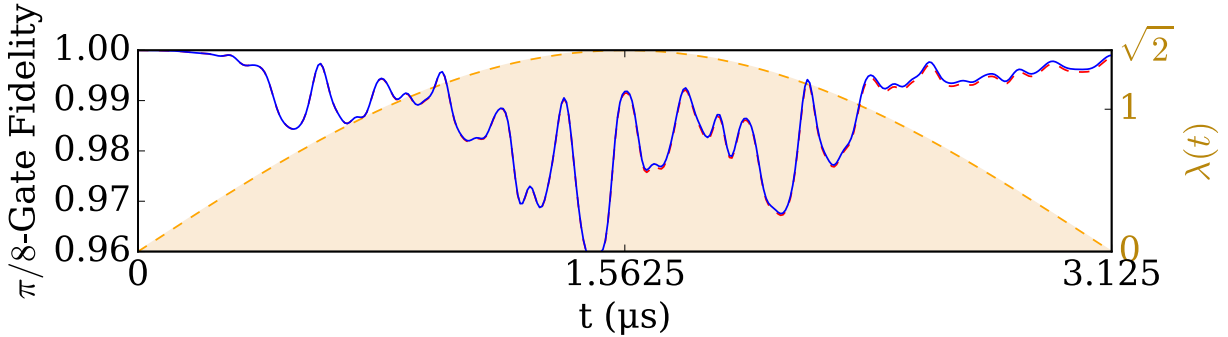


FIG. S1. Fidelity during the $\pi/8$ -gate operation by (a) abruptly turning on the PND drive with $\lambda(t) = 1$ and (b) smoothly turning on and off the PND drive with $\lambda_{\text{gate}}(t) = \sqrt{2}\sin(\pi t/T_G)$. The simulated fidelity between the states evolved by the PND drive and the states evolved by the target Hamiltonian H_Z as a function of time is shown in blue (without ancilla qubit relaxation) and red (with ancilla qubit relaxation) curves. The ramping function $\lambda(t)$ is presented as the filled orange curve. Here we use the parameters in table S5 and assume $\Gamma_q/2\pi = 3$ kHz and $T_G = 16\pi/\chi = 3.125$ μs . The initial state is $\frac{1}{\sqrt{2}}(|0\rangle_k + |1\rangle_k) \otimes |g\rangle$. At the end of the gate operation, the final gate fidelity is 99.93% for the abrupt drive and 99.90% for the smooth drive. The additional infidelity induced by ancilla relaxation is 0.75% for the abrupt drive and 0.55% for the smooth drive.

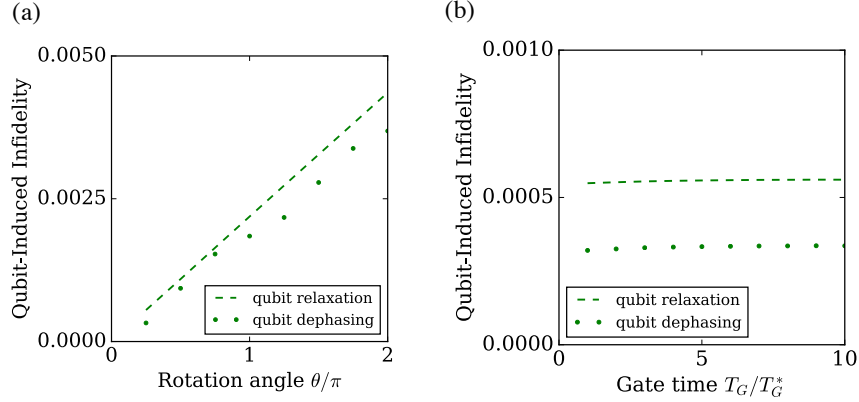


FIG. S2. Qubit-induced infidelity of the PND R_θ gate. (Values of the R_θ gate infidelity with qubit relaxation or dephasing subtracted by the gate infidelity without qubit relaxation or dephasing). (a) Qubit-induced infidelity as a function of the rotation angle θ , with fixed PND drive parameters $\chi_0, \{\Omega_0\}, \{\delta_0\}$ and with a θ -dependent gate time $T_G = (4\theta/\pi)T_G^*$. (b) Qubit-induced infidelity as a function of the gate time T_G , with fixed parameters $\theta = \pi/4, \chi_0, \{\delta_0\}$, and with T_G -dependent drive amplitudes $\{\Omega\} = \{\Omega_0\sqrt{T_G^*/T_G}\}$. Here $\chi_0, \{\Omega_0\}$, and $\{\delta_0\}$ are the parameters used in table S5. We assume $\Gamma_q/2\pi = \Gamma_\phi/2\pi = 3$ kHz, and $T_G^* = 16\pi/\chi = 3.125$ μ s. The initial state is $\frac{1}{\sqrt{2}}(|0\rangle_k + |1\rangle_k) \otimes |g\rangle$, and we assume a smooth ramping function $\lambda(t) = \sqrt{2}\sin(\pi t/T_G)$ for the drive.

II. MICROSCOPIC MODEL AND KERR CORRECTIONS

We now revisit the microscopic model of a resonator mode \hat{a} coupled to another bosonic mode \hat{d} with anharmonicity α . Specifically,

$$\hat{H} = \hbar\omega_a\hat{a}^\dagger\hat{a} + \hbar\omega_q\hat{d}^\dagger\hat{d} - \frac{\hbar\alpha}{2}\hat{d}^\dagger\hat{d}^\dagger\hat{d}\hat{d} + \hbar g(\hat{a}^\dagger\hat{d} + \hat{d}^\dagger\hat{a}). \quad (\text{S33})$$

For a small coupling g , one can use perturbation theory to estimate the frequency shifts as a function of photon number in the resonator n_a and the anharmonic mode n_d . Expanding up to the order of g^4 and keeping only $n_d = 0, 1$ (states $|g\rangle, |e\rangle$), the generic Hamiltonian of the coupled system reads

$$\begin{aligned} \hat{H} = & \hbar\left(\omega_a + \frac{g^2}{\Delta} - \frac{g^4}{\Delta^3}\right)\hat{a}^\dagger\hat{a} + \hbar\left(\omega_q - \frac{g^2}{\Delta} + \frac{g^4}{\Delta^3}\right)\hat{d}^\dagger\hat{d} - \frac{2\hbar g^2\alpha}{\Delta(\Delta + \alpha)}\hat{a}^\dagger\hat{a}\hat{d}^\dagger\hat{d} - \frac{\hbar g^4\alpha}{\Delta^3(\alpha + 2\Delta)}\hat{a}^\dagger\hat{a}^\dagger\hat{a}\hat{a} \\ & + \frac{4\hbar g^4\alpha(\alpha^2 + 2\alpha\Delta + 2\Delta^2)}{\Delta^3(\Delta + \alpha)^3}\hat{a}^\dagger\hat{a}\hat{d}^\dagger\hat{d} + \frac{\hbar g^4 2\alpha^2(3\alpha^3 + 11\alpha^2\Delta + 15\alpha\Delta^2 + 9\Delta^3)}{\Delta^3(\alpha + \Delta)^3(\alpha + 2\Delta)(3\alpha + 2\Delta)}\hat{a}^\dagger\hat{a}^\dagger\hat{a}\hat{a}\hat{d}^\dagger\hat{d} + \mathcal{O}(g^6). \end{aligned} \quad (\text{S34})$$

Here $\Delta = \omega_a - \omega_q$.

Consider an off-resonantly driven coupled system with the photon self-Kerr K and the second-order dispersive shift χ' ,

$$\begin{aligned} \hat{H}(t) = & \hbar\omega_a\hat{a}^\dagger\hat{a} + \hbar\omega_q|e\rangle\langle e| - \hbar\chi\hat{a}^\dagger\hat{a}|e\rangle\langle e| - \frac{\hbar K}{2}\hat{a}^\dagger\hat{a}^\dagger\hat{a}\hat{a} + \frac{\hbar\chi'}{2}\hat{a}^\dagger\hat{a}^\dagger\hat{a}\hat{a}|e\rangle\langle e| + \hbar\Omega(t)\hat{\sigma}_- + \hbar\Omega^*(t)\hat{\sigma}_+ \\ \equiv & \hat{H}_0 + \hat{H}_K + \hbar\Omega(t)\hat{\sigma}_- + \hbar\Omega^*(t)\hat{\sigma}_+, \end{aligned}$$

here $\Omega(t) = \sum_m \Omega_m e^{i(\omega_q - m\chi + \delta_m)t}$.

We again assume a tri-partition ansatz for the time-evolution operator,

$$\hat{U}_S(t_f, t_i) = e^{-i\hat{G}(t_f)} e^{-i\hat{H}_{\text{eff}}(t_f - t_i)/\hbar} e^{i\hat{G}(t_i)}, \quad (\text{S35})$$

and move to the interaction picture with the unitary transformation $\hat{U} = \exp\left(i(\hat{H}_0 + \hat{H}_K)t/\hbar\right)$, we are left with the drive term

$$\hat{V}_I(t) = \sum_m \sum_n \hbar(\Omega_m e^{i((n-m)\chi + \delta_m - \chi'n(n-1)/2)t} |n\rangle \langle n| \hat{\sigma}_- + H.c.). \quad (\text{S36})$$

We can again use the time-dependent perturbation theory to calculate $\hat{U}_I(t_f, t_i)$ in powers of \hat{V}_I and find the perturbative expansions $\hat{H}_{\text{eff}} = \hat{H}_{\text{eff}}^{(0)} + \hat{H}_{\text{eff}}^{(1)} + \hat{H}_{\text{eff}}^{(2)} + \dots$ and $\hat{G}_I(t) = \hat{G}_I^{(0)}(t) + \hat{G}_I^{(1)}(t) + \hat{G}_I^{(2)}(t) + \dots$, with additional contributions from the Kerr term $\hat{H}_K = \frac{\hbar K}{2} \hat{a}^\dagger \hat{a}^\dagger \hat{a} \hat{a} + \frac{\hbar K'}{2} \hat{a}^\dagger \hat{a}^\dagger \hat{a} \hat{a} |e\rangle \langle e|$.

For the zeroth order, we have $\hat{G}_I^{(0)}(t) = 0$ and $\hat{H}_{\text{eff}}^{(0)} - \hat{H}_0 = 0$. For $\mathcal{O}(\hat{V})$,

$$\hat{H}_{\text{eff}}^{(1)} = 0, \quad (\text{S37})$$

$$\hat{G}_I^{(1)}(t) = \sum_m \sum_n \frac{\Omega_m |n\rangle \langle n| \hat{\sigma}_- e^{i((n-m)\chi - \chi'n(n-1)/2 + \delta_m)t}}{i((n-m)\chi - \chi'n(n-1)/2 + \delta_m)} + H.c.. \quad (\text{S38})$$

For $\mathcal{O}(\hat{V}^2)$, We find

$$\hat{H}_{\text{eff}}^{(2)} = - \sum_m \sum_n \frac{\hbar |\Omega_m|^2 |n\rangle \langle n|}{(n-m)\chi - \chi'n(n-1)/2 + \delta_m} \hat{\sigma}_z, \quad (\text{S39})$$

$$\hat{G}_I^{(2)} = - \sum_{m_1} \sum_{m_2 \neq m_1} \sum_n \frac{\Omega_{m_1} \Omega_{m_2}^* |n\rangle \langle n| \hat{\sigma}_z e^{i(\delta_{m_1} - \delta_{m_2} - (m_1 - m_2)\chi)t}}{2i((n-m_1)\chi - \chi'n(n-1)/2 + \delta_{m_1})(\delta_{m_1} - \delta_{m_2} - (m_1 - m_2)\chi)} + H.c. \quad (\text{S40})$$

The third- and fourth-order terms in the effective Hamiltonian are

$$\hat{H}_{\text{eff}}^{(3)} = 0, \quad (\text{S41})$$

$$\begin{aligned} \hat{H}_{\text{eff}}^{(4)} = & \sum_{m_1} \sum_{m_2} \sum_n \frac{\hbar |\Omega_{m_1}|^2 |\Omega_{m_2}|^2 |n\rangle \langle n| \hat{\sigma}_z}{((n-m_1)\chi + \delta_{m_1} - \chi'n(n-1)/2)((n-m_2)\chi - \chi'n(n-1) + \delta_{m_2})^2} \\ & - \sum_{m_1} \sum_{m_2 \neq m_1} \sum_n \frac{\hbar |\Omega_{m_1}|^2 |\Omega_{m_2}|^2 |n\rangle \langle n| \hat{\sigma}_z}{((n-m_1)\chi - \chi'n(n-1)/2 + \delta_{m_1})^2 (\delta_{m_1} - \delta_{m_2} - (m_1 - m_2)\chi)} \\ & + \frac{\sum_{m_1, m_2, m_3, m_4} \sum_n \hbar \Omega_{m_1} \Omega_{m_2}^* \Omega_{m_3} \Omega_{m_4}^* |n\rangle \langle n| \hat{\sigma}_z}{((n-m_4)\chi - \chi'n(n-1)/2 + \delta_{m_4})(\delta_{m_1} - \delta_{m_2} - (m_1 - m_2)\chi)((n-m_1)\chi - \chi'n(n-1)/2 + \delta_{m_1})}, \end{aligned} \quad (\text{S42})$$

where the last term satisfies the condition $\delta_{m_1} - m_1\chi + \delta_{m_3} - m_3\chi = \delta_{m_2} - m_2\chi + \delta_{m_4} - m_4\chi$, and $m_1 \neq m_2 \neq m_3 \neq m_4$ or $m_1 = m_3 \neq m_2 \neq m_4$ or $m_2 = m_4 \neq m_1 \neq m_3$,

A. Optimized PND Parameters with Kerr and additional simulations

In this subsection we show tables of optimized PND Hamiltonian engineering parameters with the additional Kerr term. All the engineered frequency shifts are subject to a Fourier transformation precision of ± 0.5 kHz.

Additional simulations of the cat state evolution under PND Kerr cancellation is shown in Fig. S3 and S4. We assume the system starts with an even cavity cat state $\frac{1}{\sqrt{2}}(|\alpha_c\rangle + |-\alpha_c\rangle)$ and the qubit in its ground state then simulate the state evolution in the rotating frame with $\hat{U} = \exp(i(\omega_a \hat{a}^\dagger \hat{a} + \omega_q |e\rangle \langle e|)t)$. With PND Kerr cancellation, the cat state is preserved at a high fidelity $\approx 99.2\%$ even after a long time $t = 100 \mu\text{s}$. In Fig. S5 and S6 we study the micromotion and the qubit-induced infidelity for PND Kerr cancellation. We find that the amplitude of the micromotion and the qubit-induced infidelity both scale as Ω^2/χ^2 as predicted. Note that we use Kerr cancellation with $\chi' = 2K$ as a special case such that both the cavity self-Kerr and the second-order dispersive shift are cancelled out by the engineered Hamiltonian and thus there is a perfect micromotion periodicity T_M unperturbed by the total energy.

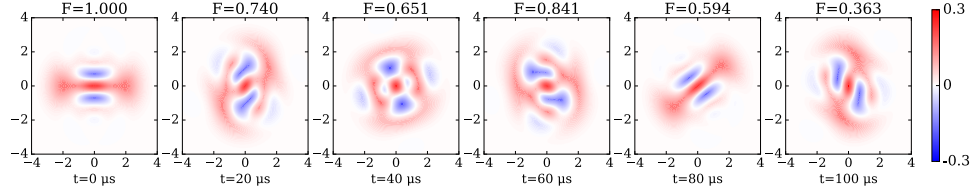
TABLE S7. Kerr Cancellation: $\chi/2\pi = 2$ MHz, $K/2\pi = 3$ kHz, $\chi'/2\pi = 6$ kHz (maintext FIG.2(b-c))

photon number	n=0	n=1	n=2	n=3	n=4	n=5	n=6
$E_{T,n}/2\pi$ (kHz)	0	0	3	9	18	30	45
$E_n/2\pi$ (kHz)	0	0	3	9	18	30.25	46.25
δ_n/χ	1/2	1/2	1/2	1/2	1/2	1/4	1/4
Ω_n/χ	0.0883	0.0658	0.0635	0.0639	0.0620	0.0534	0.0606

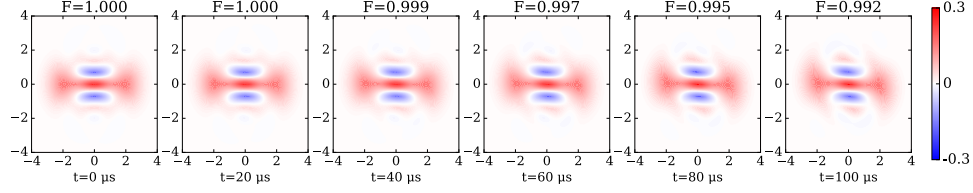
TABLE S8. Error-Transparent Z-rotation with Kerr Cancellation: $\chi/2\pi = 2$ MHz, $g_R = 20$ kHz, $K/2\pi = 3$ kHz, $\chi'/2\pi = 6$ kHz

photon number	n=0	n=1	n=2	n=3	n=4	n=5	n=6
$E_{T,n}/2\pi$ (kHz)	20	-20	-17	29	38	10	25
$E_n/2\pi$ (kHz)	20	-20	-17	29	38	9	24
δ_n/χ	1/2	- 1/2	-1/4	1/2	1/4	1/2	1/2
Ω_n/χ	0.0949	0.0659	0.0344	0.0838	0.0588	0.0257	0.0527

(a) Cat state evolution under cavity self-Kerr



(b) Cat state evolution under PND Kerr cancellation



(c) Cat state evolution under PND Kerr cancellation with lossy ancilla

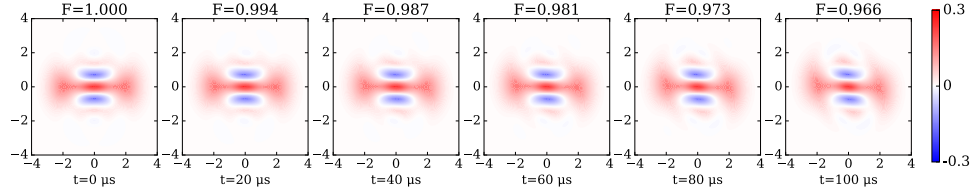
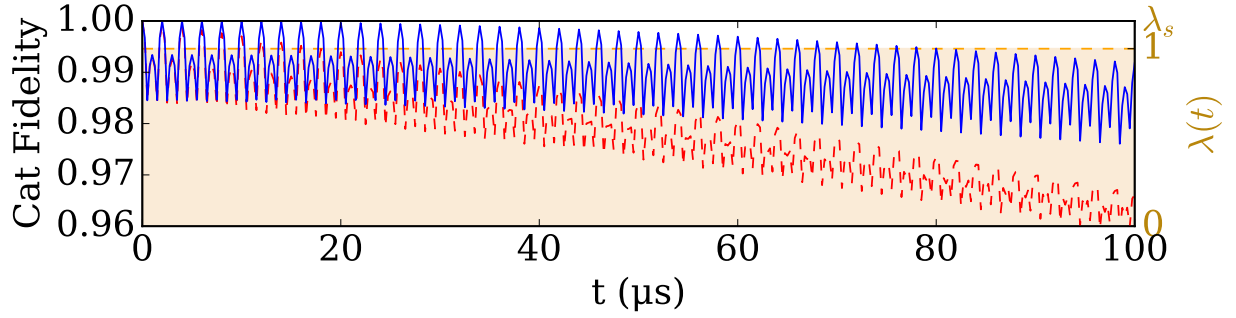


FIG. S3. Wigner function snapshots and cat fidelities under (a) cavity self-Kerr, (b) PND Kerr cancellation, and (c) PND Kerr cancellation with a lossy ancilla qubit. Here we apply abrupt PND drive with parameters shown in table S7, and assume a qubit relaxation rate $\Gamma_q/2\pi = 3$ kHz and a cat size $\alpha_c = \sqrt{2}$. The snapshots are chosen at multiples of the micromotion period $T_M = 8\pi/\chi = 2 \mu\text{s}$.

(a) abrupt drive



(b) smooth drive

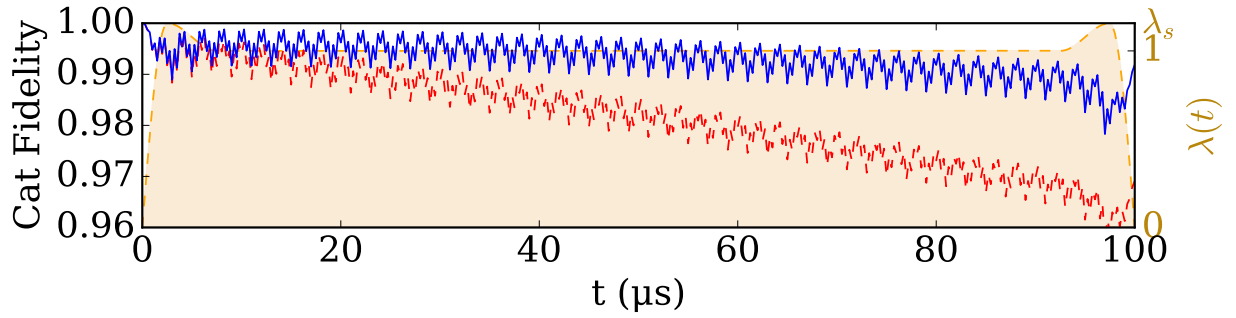


FIG. S4. Cat state fidelity during the Kerr cancellation operation by (a) abruptly turning on the PND drive and (b) smoothly turning on and off the PND drive as describe in Eq. (S18) and (S19). The cat fidelity as a function of time is shown in blue (without ancilla qubit relaxation) and red (with ancilla qubit relaxation) curves. The ramping function $\lambda(t)$ in presented as the filled orange curve. Here we use parameters shown in table S7, and assume $\Gamma_q/2\pi = 3$ kHz, $\alpha_c = \sqrt{2}$, and $T_s = 2.5 \mu\text{s}$. At the end of the operation, the final cat fidelity is 99.180% for the abrupt drive and 99.184% for the smooth drive. The additional infidelity induced by ancilla relaxation is 0.289% for the abrupt drive and 0.205% for the smooth drive. The smooth ramping scheme reduces the qubit-induced dephasing as predicted. Note that in the middle of the operation (after the ramp-up period and before the ramp-down period), the cat state fidelity is higher for the case of abrupt drive at each micromotion period because the final kick is canceled out by the initial kick.

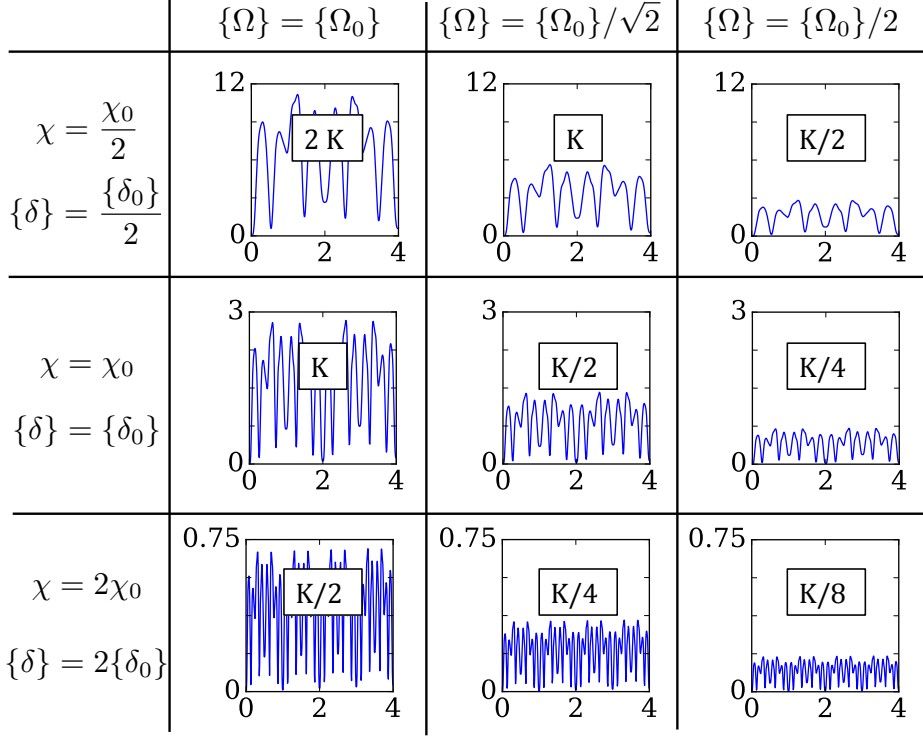


FIG. S5. Micromotion of the cat state infidelity under PND Kerr cancellation. In this table of plots we show the infidelity (x-axis, %) of a cat state (cat size $\alpha_c = \sqrt{2}$) as a function of time (y-axis, μs) with varying sets of parameters χ , $\{\Omega\}$, and $\{\delta\}$. The insets indicate the corresponding cavity self-Kerr value with $K/2\pi = 3$ kHz. Here we assume abrupt PND drive $\lambda(t) = 1$, χ_0 , $\{\Omega_0\}$, and $\{\delta_0\}$ are the parameters used in table S7. One can clearly infer that the micromotion amplitude scales as $|\Omega^2/\chi^2|$ and that the micromotion period is $T_M = 8\pi/\chi$ as predicted.

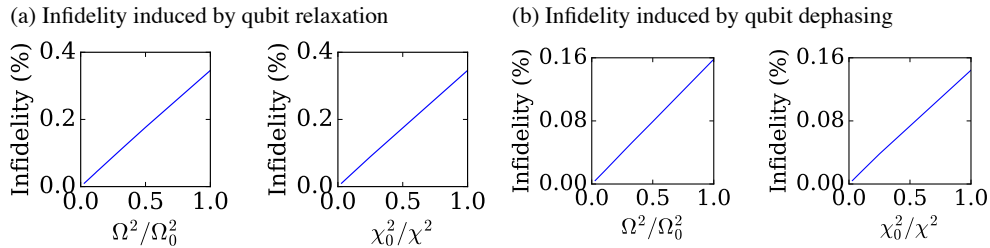


FIG. S6. Cat infidelity induced by ancilla qubit errors during PND Kerr cancellation. (a) Values of cat infidelity at time $t = 12 \mu s$ with qubit relaxation at a rate $\Gamma_q/2\pi = 3$ kHz subtracted by the cat infidelity without qubit relaxation. The left panel has a fixed $\Omega = \Omega_0$ with varying χ , and the right panel has a fixed $\chi = \chi_0$ with varying Ω . (b) Values of cat infidelity at time $t = 12 \mu s$ with qubit dephasing at a rate $\Gamma_\phi/2\pi = 3$ kHz subtracted by the cat infidelity without qubit dephasing. The left panel has a fixed $\Omega = \Omega_0$ with varying χ , and the right panel has a fixed $\chi = \chi_0$ with varying Ω . Here we assume abrupt PND drive $\lambda(t) = 1$, χ_0 , $\{\Omega_0\}$, and $\{\delta_0\}$ are the parameters used in table S7, $K/2\pi = (\Omega^2\chi_0/\Omega_0^2\chi)3$ kHz, and a cat size $\alpha_c = \sqrt{2}$.

III. HAMILTONIAN ENGINEERING FOR TWO COUPLED CAVITIES

Consider two cavity modes \hat{a} and \hat{b} dispersively coupled to two ancilla qubits $\hat{\sigma}^a$ and $\hat{\sigma}^b$ respectively, and to another qubit $\hat{\sigma}^c$ jointly with a dispersive shift χ_c , assumed to be equal for both modes,

$$\begin{aligned} \hat{H}_0 = & \hbar\omega_a \hat{a}^\dagger \hat{a} + \hbar\omega_{q,a} |e_a\rangle \langle e_a| - \hbar\chi_a \hat{a}^\dagger \hat{a} |e_a\rangle \langle e_a| + \hbar\omega_b \hat{b}^\dagger \hat{b} + \hbar\omega_{q,b} |e_b\rangle \langle e_b| - \hbar\chi_b \hat{b}^\dagger \hat{b} |e_b\rangle \langle e_b| \\ & + \hbar\omega_{q,c} |e_c\rangle \langle e_c| - \hbar\chi_c (\hat{a}^\dagger \hat{a} + \hat{b}^\dagger \hat{b}) |e_c\rangle \langle e_c|. \end{aligned} \quad (\text{S43})$$

We can add a drive term

$$\hat{H}_d(t) = \hbar\Omega_a(t) \hat{\sigma}_-^a + \hbar\Omega_a^*(t) \hat{\sigma}_+^a + \hbar\Omega_b(t) \hat{\sigma}_-^b + \hbar\Omega_b^*(t) \hat{\sigma}_+^b + \hbar\Omega_c(t) \hat{\sigma}_-^c + \hbar\Omega_c^*(t) \hat{\sigma}_+^c \quad (\text{S44})$$

with $\Omega_a(t) = \sum_{m_a} \Omega_{m_a} e^{i(\omega_{q,a} - m_a \chi_a + \delta_{m_a})t}$, $\Omega_b(t) = \sum_{m_b} \Omega_{m_b} e^{i(\omega_{q,b} - m_b \chi_b + \delta_{m_b})t}$, and $\Omega_c(t) = \sum_{m_c} \Omega_{m_c} e^{i(\omega_{q,c} - m_c \chi_c + \delta_{m_c})t}$ to engineer Hamiltonian for the two coupled cavities, assuming $|\Omega_{m_i}| \ll \chi_i, |\delta_{m_i}|$, $i = a, b, c$. Specifically, the effective Hamiltonian will be of the form $\hat{H}_{\text{eff}} = \hat{H}_{\text{eff}}^{(a)} + \hat{H}_{\text{eff}}^{(b)} + \hat{H}_{\text{eff}}^{(c)}$ with second order terms

$$\hat{H}_{\text{eff}}^{(a,2)} = - \sum_{m_a} \sum_{n_a} \frac{\hbar |\Omega_{m_a}|^2 |n_a\rangle \langle n_a|}{(n_a - m_a) \chi_a + \delta_{m_a}} \hat{\sigma}_z^a, \quad (\text{S45})$$

$$\hat{H}_{\text{eff}}^{(b,2)} = - \sum_{m_b} \sum_{n_b} \frac{\hbar |\Omega_{m_b}|^2 |n_b\rangle \langle n_b|}{(n_b - m_b) \chi_b + \delta_{m_b}} \hat{\sigma}_z^b, \quad (\text{S46})$$

$$\hat{H}_{\text{eff}}^{(c,2)} = - \sum_{m_c} \sum_{n_a} \sum_{n_b} \frac{\hbar |\Omega_{m_c}|^2 |n_a, n_b\rangle \langle n_a, n_b|}{(n_a + n_b - m_c) \chi_c + \delta_{m_c}} \hat{\sigma}_z^c. \quad (\text{S47})$$

The fourth order terms can be found as in section I. The engineered Hamiltonian is

$$\begin{aligned} \hat{H}_E = & \langle g_a g_b g_c | \hat{H}_{\text{eff}} | g_a g_b g_c \rangle = \sum_{n_a, n_b} \hbar E_{n_a n_b} |n_a n_b\rangle \langle n_a n_b| = \sum_{n_a, n_b} \hbar (E_{c, n_a + n_b} + E_{a, n_a} + E_{b, n_b}) |n_a n_b\rangle \langle n_a n_b| \\ \approx & \sum_{m_a} \sum_{n_a} \frac{\hbar |\Omega_{m_a}|^2 |n_a\rangle \langle n_a|}{(n_a - m_a) \chi_a + \delta_{m_a}} + \sum_{m_b} \sum_{n_b} \frac{\hbar |\Omega_{m_b}|^2 |n_b\rangle \langle n_b|}{(n_b - m_b) \chi_b + \delta_{m_b}} + \sum_{m_c} \sum_{n_a} \sum_{n_b} \frac{\hbar |\Omega_{m_c}|^2 |n_a, n_b\rangle \langle n_a, n_b|}{(n_a + n_b - m_c) \chi_c + \delta_{m_c}}. \end{aligned} \quad (\text{S48})$$

A. Error-transparent controlled-Z-rotation

The form of the engineered Hamiltonian does not have the full degree of freedom to create arbitrary structure of $E_{n_a n_b}$ but is enough to design error-transparent controlled-rotation along the Z axis for implementing CPHASE gate on rotational-symmetric bosonic codes. Specifically, by solving for target frequency shifts

$$E_{T, n_a} = \begin{cases} g_c R / 4 & n_a \bmod (2d_{n_a}) = 0, 2d_{n_a} - 1, \dots, d_{n_a} + 1 \\ -g_c R / 4 & n_a \bmod (2d_{n_a}) = d_{n_a}, d_{n_a} - 1, \dots, 1 \end{cases}, \quad (\text{S49})$$

which takes $\{I, \hat{a}, \dots, \hat{a}^{d_{n_a}-1}\} |0_a\rangle_L \rightarrow e^{-ig_{cR}t/4} \{I, \hat{a}, \dots, \hat{a}^{d_{n_a}-1}\} |0_a\rangle_L$ and $\{I, \hat{a}, \dots, \hat{a}^{d_{n_a}-1}\} |1_a\rangle_L \rightarrow e^{ig_{cR}t/4} \{I, \hat{a}, \dots, \hat{a}^{d_{n_a}-1}\} |1_a\rangle_L$,

$$E_{T,n_b} = \begin{cases} g_{cR}/4 & n_b \bmod (2d_{n_b}) = 0, 2d_{n_b} - 1, \dots, d_{n_b} + 1 \\ -g_{cR}/4 & n_b \bmod (2d_{n_b}) = d_{n_b}, d_{n_b} - 1, \dots, 1 \end{cases}, \quad (\text{S50})$$

which takes $\{I, \hat{b}, \dots, \hat{b}^{d_{n_b}-1}\} |0_b\rangle_L \rightarrow e^{-ig_{cR}t/4} \{I, \hat{b}, \dots, \hat{b}^{d_{n_b}-1}\} |0_b\rangle_L$ and $\{I, \hat{b}, \dots, \hat{b}^{d_{n_b}-1}\} |1_b\rangle_L \rightarrow e^{ig_{cR}t/4} \{I, \hat{b}, \dots, \hat{b}^{d_{n_b}-1}\} |1_b\rangle_L$, and

$$E_{T,n_a+n_b} = \begin{cases} -g_{cR}/2 & n_a + n_b \bmod (d_{n_a} + d_{n_b}) = 0, d_{n_a} + d_{n_b} - 1, \dots, d_{n_a} + d_{n_b} - d_n + 1 \\ 0 & \text{otherwise} \end{cases}, \quad (\text{S51})$$

which takes $\{I, \hat{a}^{l_a} \hat{b}^{l_b}\} |0_a 0_b\rangle_L \rightarrow e^{ig_{cR}t/2} \{I, \hat{a}^{l_a} \hat{b}^{l_b}\} |0_a 0_b\rangle_L$, $\{I, \hat{a}^{l_a} \hat{b}^{l_b}\} |0_a 1_b\rangle_L \rightarrow \{I, \hat{a}^{l_a} \hat{b}^{l_b}\} |0_a 1_b\rangle_L$, $\{I, \hat{a}^{l_a} \hat{b}^{l_b}\} |1_a 0_b\rangle_L \rightarrow \{I, \hat{a}^{l_a} \hat{b}^{l_b}\} |1_a 0_b\rangle_L$, and $\{I, \hat{a}^{l_a} \hat{b}^{l_b}\} |1_a 1_b\rangle_L \rightarrow e^{ig_{cR}t/2} \{I, \hat{a}^{l_a} \hat{b}^{l_b}\} |1_a 1_b\rangle_L$ for all $l_a = 0, 1, \dots, d_n - 1$ and $l_b = 0, 1, \dots, d_n - 1 - l_a$. Within a total number distance $d_n = \min(d_{n_a}, d_{n_b})$, the overall Hamiltonian should accumulate the same phase for $|1_a 1_b\rangle_L$ and its error states while keeping $|0_a 0_b\rangle_L$, $|0_a 1_b\rangle_L$, $|1_a 0_b\rangle_L$ and their error states unchanged.

Below we show tables of optimized parameters for implementing such error-transparent controlled-rotation with $d_{n_a} = d_{n_b} = d_n = 2$. All the engineered frequency shifts are subject to a Fourier transformation precision of ± 0.5 kHz.

TABLE S9. Error-Transparent Controlled-Rotation (drives on qubit $\hat{\sigma}^a$): $\chi_a/2\pi = 2.56$ MHz

photon number	$n_a=0$	$n_a=1$	$n_a=2$	$n_a=3$	$n_a=4$
$E_{T,n_a}/2\pi$ (kHz)	5	-5	-5	5	5
$E_{a,n_a}/2\pi$ (kHz)	5	-5	-5	5	5
δ_{n_a}/χ	1/2	-1/4	-1/2	-1/2	-1/2
Ω_{n_a}/χ	0.0393	0.0212	0.0365	0.0243	0.0175

TABLE S10. Error-Transparent Controlled-Rotation (drives on qubit $\hat{\sigma}^b$): $\chi_b/2\pi = 2.56$ MHz

photon number n_b	$n_b=0$	$n_b=1$	$n_b=2$	$n_b=3$	$n_b=4$
$E_{T,n_b}/2\pi$ (kHz)	5	-5	-5	5	5
$E_{b,n_b}/2\pi$ (kHz)	5	-5	-5	5	5
δ_{n_b}/χ	1/2	-1/4	-1/2	-1/2	-1/2
Ω_{n_b}/χ	0.0393	0.0212	0.0365	0.0243	0.0175

TABLE S11. Error-Transparent Controlled-Rotation (drives on qubit $\hat{\sigma}^c$): $\chi_c/2\pi = 2.56$ MHz

photon number $n_c = n_a + n_b$	$n_c=0$	$n_c=1$	$n_c=2$	$n_c=3$	$n_c=4$	$n_c=5$	$n_c=6$	$n_c=7$	$n_c=8$
$E_{T,n_b}/2\pi$ (kHz)	-10	0	0	-10	-10	0	0	-10	-10
$E_{b,n_b}/2\pi$ (kHz)	-10	0	0	-10	-10	0	0	-10	-10
δ_{n_b}/χ	-1/2	1/4	1/2	-1/4	-1/2	-1/4	-1/4	-1/2	-1/2
Ω_{n_b}/χ	0.0280	0.0197	0.0268	0.0245	0.0421	0.0257	0.00486	0.0379	0.0633

-
- [1] M. Boissonneault, J. M. Gambetta, and A. Blais, *Phys. Rev. A* **79**, 013819 (2009).
[2] S. Rahav, I. Gilary, and S. Fishman, *Phys. Rev. A* **68**, 013820 (2003).
[3] N. Goldman and J. Dalibard, *Phys. Rev. X* **4**, 031027 (2014).
[4] C. M. Dai, Z. C. Shi, and X. X. Yi, *Phys. Rev. A* **83**, 032121 (2016).
[5] S. Scopa, G. T. Landi, A. Hammoumi, and D. Karevski, *Phys. Rev. A* **99**, 022105 (2019).